A SEMI-MICROSCOPIC CALCULATION OF THE POTENTIAL IN
HEAVY ION COLLISIONS

by

David Athol Saloner

A Dissertation Submitted to the Faculty of
Science, University of the Witwatersrand, Johannesburg
for the degree of Master of Science.

Johannesburg
March 1975

ACKNOWLEDGEMENTS

I wish to express here my appreciation to those people
who have given me assistance and support in this work.

To my supervisor Professor C. Toepffer, who suggested
this project, go my sincere thanks for the assistance and
encouragement he has given me. He has given freely of
his time and always shown a keen interest in my work.

Professor J.P.F. Sellschop, my co-supervisor and
Director of the Nuclear Physics Research Unit, always made
himself available to discuss any difficulties that I had
encountered. I am indebted to him for his unfailing support.

I thank my parents for their confidence, encouragement
and support.

To my colleagues in the Nuclear Physics Research Unit
goes my appreciation for their willingness to assist me in
overcoming those problems which arose in my work.   In
particular I would like to thank those members of the Unit
and the members of the Computer Centre who gave me
invaluable assistance with computing problems.   I would
further like to thank the Computer Centre for the generous
amount of time given to me on the IBM 370/145.

I would like to thank Miss A. Cameron for the care
and patience she has shown in typing this thesis.

Finally I would like to thank the University of the
Witwatersrand for the senior bursary which I held during
the period of this work.

CONTENTS

CHAPTER I

Introduction

The development of accelerators able to produce high
energy heavy-ion beams with high energy resolution and
convenient energy variability has been responsible for an
upsurge of both experimental and theoretical activity in
the field of heavy-ion physics.

In comparison with single nucleon induced reactions,
heavy-ion processes involve a much larger number of reaction
channels because of the complex nature of the interactions
involving the possibility of high energy and momentum transfer.
One of the more exciting aspects in the study of these
processes is the possibility of gaining insight into fusion
reactions leading to the creation of superheavy elements.

The nature of the heavy-ion process depends strongly
on whether the incident ion is able to probe the nuclear
forces of the target ion. The nuclear forces are short-
ranged and are only effective when the separation of the
nuclei is less than the sum, R_c, of the radii of the charge
distributions of the interacting ions.

$$R_C = R_{C1} + R_{C2} = r_o(A_1^{1/3} + A_2^{1/3}) \tag{1.1}$$

Therefore the nature of the process will change when
the total kinetic energy of the interaction in the centre-of-
mass system becomes larger than the Coulomb barrier E_c.

$$E_o = \frac{Z_1 Z_2 e^2}{R_o} \qquad\qquad (1.2)$$

where the incident nucleus has charge $Z_1 e$

and the target nucleus has charge $Z_2 e$.

For interactions with energies below this barrier only Coulomb scattering takes place. For example, in the elastic scattering of 27 MeV ^{16}O ions on ^{197}Au the angular distribution has a pure Rutherford form (Fig. 1.1) :
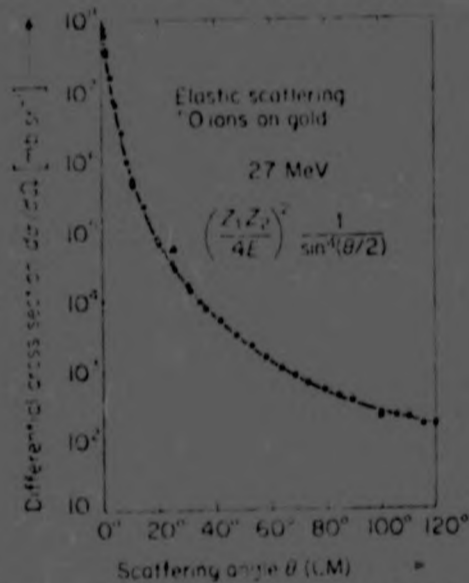
Fig. 1.1. Pure Rutherford-type elastic scattering of 27-MeV ^{16}O ions on gold.

However at higher energies the nuclear forces are probed and large deviations from pure Coulomb scattering predictions are observed (Fig. 1.2) :

.
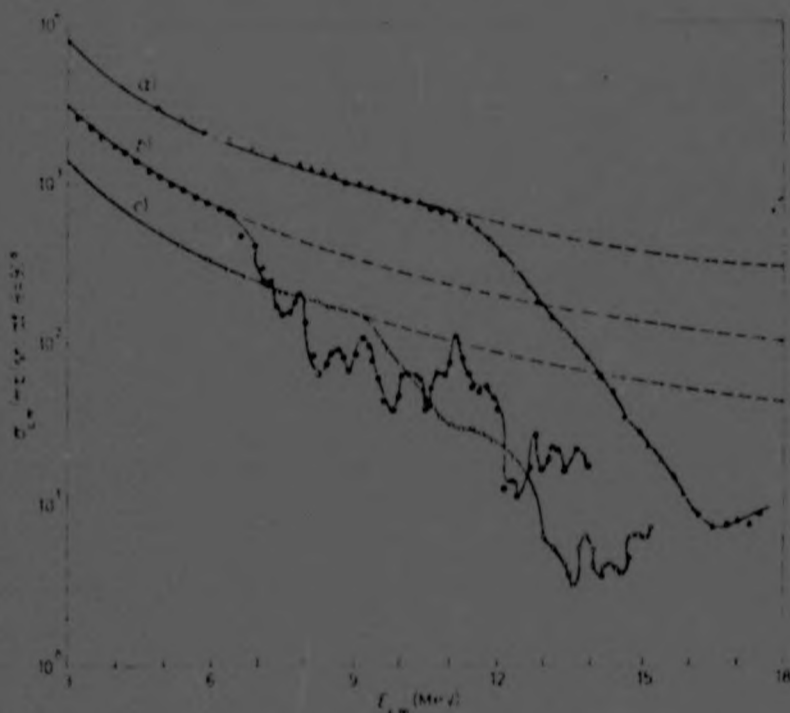
Fig. 1.2. Excitation functions for three different reactions. Curves
a), b) and c) refer to the cross-sections for $^{16}O+^{16}O$, $^{12}C+^{12}C$ and
$^{16}O+^{12}C$ respectively. Dashed lines represent the classical Mott
formula for the pure Coulomb scattering.

a) $E_c=13.5$ MeV. b) $E_c=8.5$ MeV, c) $E_c=10.5$ MeV.

The criterion for classical behaviour is that the
Sommerfeld parameter, η, must be greater than unity, i.e.

$$\eta = \frac{Z_1 Z_2 e^2}{\hbar v} > 1 \tag{1.3}$$

If $\eta>1$ the particle orbits can be taken to be pure
Rutherford orbits.

When the projectile and target particles are identical
nuclei we expect the Mott scattering predictions to be
fulfilled. We expect oscillations in the cross-sections to
be present and, because of the indistinguishability of
scattered and recoil particles, to have symmetry about
$\theta=90^\circ$ in the centre-of-mass system. Figs. 1.3a-e show how
this is observed for $^{16}O-^{16}O$ scattering and the deviations
from the Mott predictions at energies above the Coulomb

barrier (E_c = 10.5 MeV).
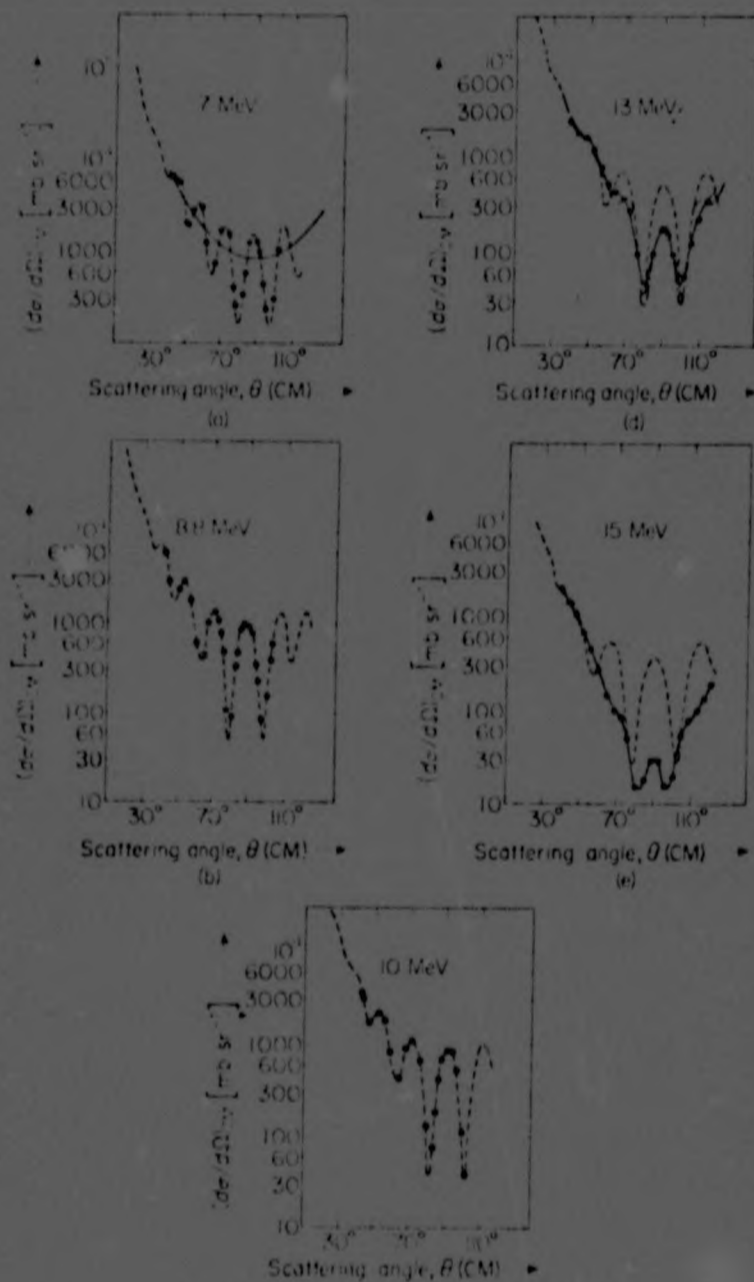
Fig. 1.3 The $^{16}O+^{16}O$ system at energies between 7 and 15 MeV (the corresponding Coulomb energy is E_c = 10.5 MeV).

The observed analogy between the behaviour of the excitation functions for heavy-ion collisions and the observed diffraction effects in classical optics initially led to a focus of interest on the explanation of heavy-ion collisions in terms of semi-classical methods. In Chapter II the application of diffraction techniques to the

heavy-ion scattering problem is discussed.

However for a better insight into the underlying many-body problem one would like to develop models which show an explicit dependance on quantities such as the value of the relative coordinate and for which a Schrodinger equation can be formulated and solved. This led to the development of optical potentials for these reactions. The concept of a nuclear molecule increased interest in the development of such models. The first potentials proposed were derived from phenomenological fits and are discussed in Chapter III.

In Chapter IV the extended liquid drop model is discussed which provides a semi-microscopic foundation for the derivation of the real potential in the heavy-ion scattering process.

The extended liquid drop method treats average properties of the nucleus. In such a treatment the effects of the presence of nuclear shells is neglected. Chapter V outlines how the shell effects can be incorporated into the extended liquid drop model within the framework of a two-centre shell model.

In heavy-ion collisions the presence of intermediate structure in the excitation functions is clearly seen. Much of this structure can be explained in terms of resonances between quasibound molecules and virtual states of a quasimolecule.' The coupled channels approach, discussed in Chapter VI, explicitly allows for such effects.

Some of the approaches that have been adopted in deriving a more fundamental derivation of the imaginary potential are discussed in Chapter VII. There it is seen that there exists the possibility for a dynamic treatment of the problem using momentum space considerations. This approach provides a parameter free imaginary potential.

Chapter VIII deals with the use of the folding method to derive the form of the real potential. Various forms for the nucleon-nucleon interaction are postulated and corresponding nucleus-nucleus potentials derived.

The treatments outlined up till Chapter VIII lack a convincing microscopic model of the real potential having an energy dependance and no free parameters. In Chapter IX an energy dependant, parameter free real potential is developed from momentum space considerations. The potential is derived in the two extreme cases of adiabatic and sudden approximation. This real potential is used along with the parameter free, energy dependant imaginary potential described in Chapter VII to predict the cross-section for $^{16}O-^{16}O$ scattering.

CHAPTER II

Diffraction models.

II.1 Introduction

At energies above the Coulomb barrier the form of the
angular dependance and the gross structure of the scattering
cross-section indicates a close analogy with optical
diffraction processes.   It was for this reason that the
diffraction model was among the earliest models put
forward to understand the nature of the interaction in
heavy-ion collisions.   By using a diffraction model it is
possible to bypass having to solve a Schrodinger equation
and to get good agreement with experiment by a suitable
variation of the parameters involved.

For low values of η the form of the cross-section is
of the type associated with Fraunhofer diffraction and for
high values of η the form is of Fresnel type.   The
transition from the one form to the other can be clearly
seen in the angular distributions of 158 MeV ^{16}O ions
elastically scattered on nuclides having progressively
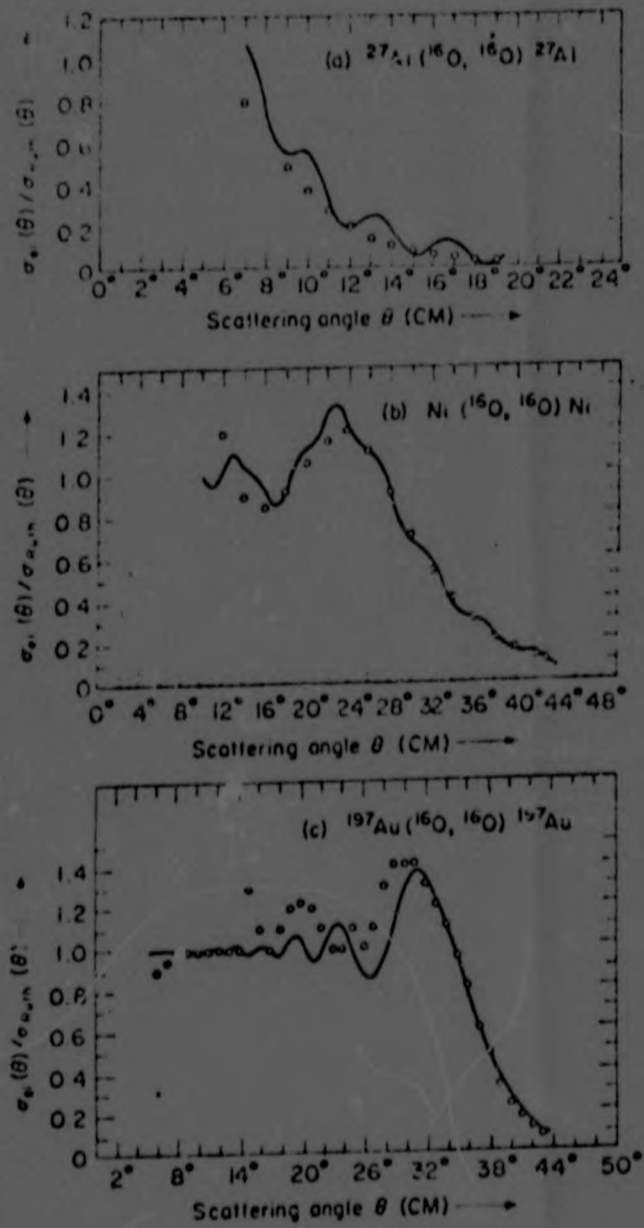higher atomic number.

Fig. 2.1. Transition from Fraunhofer-type diffraction structure to Fresnel-type, illustrated by the angular distributions of 158-MeV ^{16}O ions elastically scattered on nuclides having progressively higher atomic number. (a) Fraunhofer structure for $^{27}_{13}$Al, (b) intermediate structure for $^{58}_{28}$Ni, (c) Fresnel structure for $^{197}_{79}$Au.

Using arguments from physical optics we will investigate
the origin of these processes [1].

The basic condition for diffraction of a wave by an
opaque object is that the wavelength be small compared with
the linear dimension a of the object.   That is, we require

$$ka \gg 1$$

If d is the shorter of the two distances d_1, between source
point and object, and d_2, between observation point and
object, then

$$\frac{ka^2}{d} \ll 1 \text{ implies Fraunhofer diffraction} \qquad (2.1a)$$

$$\text{and} \quad \frac{ka^2}{d} \gtrsim 1 \text{ implies Fresnel diffraction} \qquad (2.1b)$$

Since k and a have magnitudes of the order of the size
of the nucleus and since d will be of the order of
centimetres we would expect that the second condition is
never met.   However, closer consideration of the physics of
the problem shows that this is not the case.

Consider the elastic scattering of a projectile, mass m_1,
by the Coulomb field of a spherical target nucleus, mass m_2.
The Coulomb field distorts the incoming wave such that there
is appreciable curvature of the wavefront over the region of
the nucleus.   For strongly absorbing nuclei this corresponds
to Fresnel diffraction by a black sphere.

The scattering angle for a collision as illustrated in
Fig. 2.2, is related to the impact parameter b by

$$b = \frac{n}{k} \cot \frac{\theta}{2} \qquad (2.2)$$

For a given classical trajectory the distance of
closest approach, D, is

$$D = \frac{\eta}{k} (1 + \text{cosec } \frac{\theta}{2})$$ (2.3)

The grazing trajectory is the one for which D equals the sum, R, of the target and projectile radii and we define the critical angle θ_c as the scattering angle corresponding to that trajectory

$$R = \frac{\eta}{k} (1 + \text{cosec } \frac{\theta_c}{2})$$ (2.4)

This gives the corresponding impact parameter bc as

$$bc = \frac{\eta}{k} \cot \frac{\theta_c}{2}$$ (2.5)

Particles which are scattered through the angle θ_c appear to originate from a virtual point source at a finite distance, d, from the scattering centre and in this way condition 2.1b can be fulfilled. Large values of η correspond to small values of d and thus to Fresnel diffraction whereas small values of η correspond to large values of d and thus to Fraunhofer diffraction.
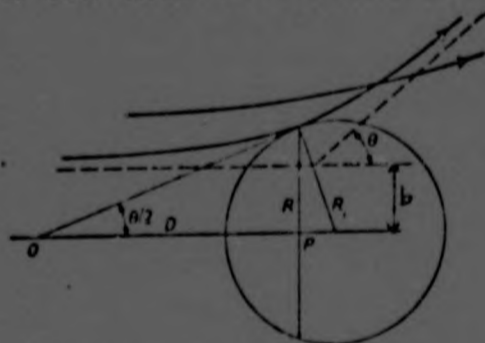

Fig. 2.2. Schematic representation of charged-particle scattering phenomenon. The circle represents the strongly absorbing sphere

One can derive a simple expression for the critical angle θ_c from equation 4, namely

$$\theta_c = \text{arctg } \frac{\eta}{\Lambda}$$ (2.6)

where Λ is an angular momentum related to R by

$$\Lambda = kR \left(1 - \frac{2\eta}{kR}\right)^{\frac{1}{2}} \qquad (2.7)$$

Using these parameters and introducing a quantity d which describes the diffuseness of the nuclear surface, we are able, using classical diffraction relations, to give a qualitative description of the scattering [2].

Firstly, we consider the scattering as a function of scattering angle. Two regions can be identified in the scattering. One, associated with $\theta < \theta c$, where Coulomb scattering dominates and the other, associated with $\theta > \theta c$, where the nuclear potential is probed.

For heavy nuclei Fresnel-type oscillations appear in the Coulomb region. In the nuclear scattering region σ/σ_R decreases monotonically with an exponential fall-off rate.

$$\theta \gg \theta c, \quad \frac{\sigma}{\sigma_R} \propto \exp\left[-2\pi\Delta(\theta-\theta c)\right] \qquad (2.8)$$

where the rate of fall-off is related to the diffuseness of the nuclear surface d, through

$$\Delta = kd \frac{1 - \eta/_{kR}}{\sqrt{ - (2\eta/_{kR})}} \qquad (2.9)$$

For light target nuclei the angle θc is relatively small and so the condition for nuclear scattering to occur is predominantly fulfilled. The decrease of σ/σ_R is still given by equation 2.8, but the fall-off is no longer monotonic. Oscillations can now arise having a period

$$\approx \pi/_\Lambda$$

with an amplitude given by

$$A(\theta) = 2 \exp (-2\pi\Delta\theta c)$$

$$= 2 \exp (-2\pi\eta\frac{d}{R}) \tag{2.10}$$

We will now consider excitation functions, i.e. the variation of the differential cross-section with the energy of the collision. We can again identify two regions for the scattering.

$$I. \quad E_B = \frac{E_c}{2} (1+\cosec \frac{\theta}{2}) \tag{2.11}$$

where E_c is the Coulomb barrier then $E > E_B$ implies that the nuclear potential is being probed and $E < E_B$ implies that the scattering is Coulomb scattering. For $E > E_B$ an exponential decrease in the scattering cross-section is predicted for heavy nuclei

$$\frac{\sigma}{\sigma_R} \sim C(\theta) \ (\frac{d}{R})^2 \ (\frac{E}{E_c})^{5/2} \ \exp \ [-2\pi\gamma\frac{d}{R}\sqrt{\frac{E}{E_c}}] \tag{2.12}$$

where $\gamma = \frac{(2Z_1 Z_2 \ e^2 \ \mu R)^{\frac{1}{2}}}{\hbar}$

and $C(\theta)$ is a function of scattering angle only. For lighter nuclei, oscillations of period T and amplitude A are predicted where T and A go as :

$$T \propto \frac{1}{\theta} \ \frac{E/E_c}{\sqrt{E/E_c - 1}} \tag{2.13}$$

$$A \sim \exp \ [-2\pi\gamma\frac{d}{R}\sqrt{\frac{E_c}{E}}] \tag{2.14}$$

The period of the oscillations can be seen to increase with increasing energy and to decrease with increasing scattering angle. The amplitude of these oscillations decrease with increasing energy and increase strongly with decreasing diffuseness of the surface.

II.2 Strong Absorption Models

Various models have been proposed to account for the scattering behaviour in general situations.   We will restrict ourselves here to the case of zero-spin particles for which the scattering amplitude is

$$f(\theta) = \frac{\lambda}{2i} \sum_{\ell=0}^{\infty} (2\ell+1) \left[\eta_\ell - 1\right] P_\ell(\cos\theta) \qquad (2.15)$$

where $\eta_\ell = \exp 2i\sigma_\ell$ and $\delta_\ell = \alpha_\ell + i\beta_\ell + \sigma_\ell$
α_ℓ describes the deviation from the Coulomb phase shift σ_ℓ arising from the nuclear contribution. β_ℓ describes the effect of absorption by the nucleus.   The Coulomb phase shifts are given by:

$$\exp 2i\sigma_\ell = \frac{\Gamma(\ell+1+i\eta)}{\Gamma(\ell+1-i\eta)} \qquad (2.16)$$

$$\eta_\ell = \exp\left[2i(\mathrm{Re}\ \delta_\ell + i\mathrm{Im}\ \delta_\ell)\right]$$

$$= A_\ell \exp\left[2i\ \mathrm{Re}\ \delta_\ell\right]$$

is the partial-wave nuclear scattering amplitude.   Now we have (eqn2.₂) that the impact parameter b is given by

$$b = \frac{Z_1 Z_2 e^2}{mv^2} \cot\left(\frac{\theta}{2}\right)$$

The classical orbital momentum of the incident particle,

$$1_{c\ell} = mvb \qquad (2.17)$$

is therefore given by

$$1_{c\ell} = \frac{Z_1 Z_2 e^2}{v} \cot\left(\frac{\theta}{2}\right) \qquad (2.18)$$

and the distance of closest approach by

$$r_{min} = \frac{Z_1 Z_2 e^2}{2E} \left(1 + \mathrm{cosec}\ \frac{\theta}{2}\right) \qquad (2.19)$$

The lower limit R, to the distance of closest
approach is reached when r_{min} = R = the sum of the particle
radii.   The corresponding critical orbital momentum ℓ',
can be given in its quantum mechanical form as

$$\hbar^2 \, \ell'(\ell'+1) = 2mR^2(E-\frac{Z_1 Z_2 e^2}{R}) \qquad (2.20)$$

One of the earliest and simplest models proposed to
account for the scattering behaviour is the sharp cut-off,
strong absorption approach known as the Blair model [3].
The basic assumption in the Blair model is that all
projectiles whose orbital momentum exceeds ℓ' pass by the
nucleus along Rutherford trajectories but all those having
an orbital momentum $\ell \leq \ell'$ are absorbed by the nucleus out
of the incident beam and do not experience elastic
scattering.   This is equivalent to excluding all particles
which would have a small impact parameter in the classical
picture and could thus conceivably cause interpenetration and
give rise not only to elastic scattering but also to
inelastic scattering.

This assumption has the effect of terminating the sum
in the cross-section expression to:

$$\sigma(\theta) = |f(\theta)|^2 = \left| \frac{\chi}{2i} \sum_{\ell=0}^{\ell'} (2\ell+1)\, (1-\eta_\ell)\, P_\ell(\cos\theta) \right|^2$$

The Blair model assumes that the nuclear forces can
only affect the scattering interaction by giving rise to an
absorption.   Therefore the real phase component α_ℓ is set to
zero.   The value of β_ℓ , the imaginary component, will
determine the absorption.   In the strong absorption model
β_ℓ is chosen such that:

$$\exp(-2\beta_\ell) = 0 \qquad \ell \leq \ell'$$

$$\exp(-2\beta_\ell) = 1 \qquad \ell > \ell' \tag{2.21}$$

i.e. $\eta_\ell = 0$ for $\ell \leq \ell'$, therefore partial waves with $\ell < \ell'$
experience pure Coulomb scattering.

This parametrization of the phases is able to bring
out the main qualitative features of the diffraction
scattering. In particular it is able to reproduce the
experimental observation that at the critical value $\ell = \ell'$,
corresponding to $r_{min} = R$, the observed elastic scattering
cross-section exceeds the Rutherford value (see Fig.2.1).
However, there is disagreement with the experimental data
in that the calculated amplitude of the oscillations is
much larger than the observed amplitude. Also, the
decrease in the calculated angular distribution is slower
than is experimentally observed.

The failure of the sharp cut-off model on these points
is not surprising. In diffraction scattering processes,
the nuclear surface plays an important role. In this
model the scattering is presumed to be insensitive to the
shape of the surface. A more realistic description of
the scattering would allow for a more gradual transition of
η_ℓ from zero to unity. This transition would extend over
a range of ℓ values in the vicinity of ℓ'. In the same
way as large oscillations arise when a Fourier series is
terminated, the strong oscillations arising from the Blair
model can be considered to arise from the sharp cut-off of
the partial waves. By effecting a more gradual cut-off
these unphysical oscillations can be damped out.

The problem, then, is to find suitable parametrizations derivation of a closed expression for the scattering cross-section. A parametrization which has met with much success is that of Frahn and Venter [4]. Their parametrization is of the form:

$$\text{Re}\,n_\ell = \exp(-2\text{Im}\delta_\ell)\,\cos(2\text{Re}\delta_\ell) = g\left(\frac{\ell'-\ell}{\Delta}\right) \tag{2.22}$$

$$\text{Im}\,n_\ell = \exp(-2\text{Im}\delta_\ell)\,\sin(2\text{Re}\delta_\ell) = \mu\frac{dg}{d\ell}\left(\frac{\ell'-\ell}{\Delta}\right)$$

Frahn and Venter were able to derive a closed and simple form for the scattering amplitude useful for the determination of the parameters by fitting the cross-sections to the experimental data. In this treatment $g\left(\frac{\ell'-\ell}{\Delta}\right)$ is a continuously differentiable function of $\left(\frac{\ell'-\ell}{\Delta}\right)$ with a first derivative symmetric and peaked at ℓ' but otherwise arbitrary. It is thus possible to apply the results of this analysis to a large variety of types of n_ℓ. The standard forms for $\text{Re}\,n_\ell$ and $\text{Im}\,n_\ell$ are shown in Fig. 2.3
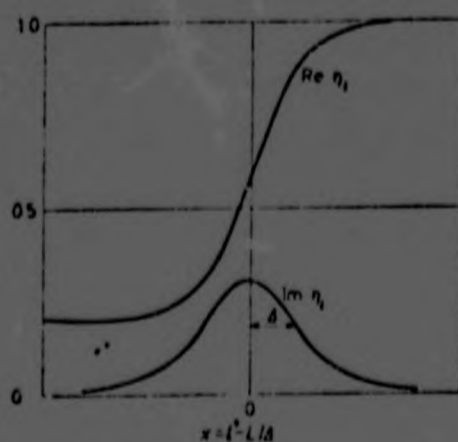
Fig. 2.3. Standard form of $\text{Re}\,n_\ell$ and $\text{Im}\,n_\ell$.

The real part of η_ℓ changes from small values at small ℓ to unity at high ℓ by a rapid transition in the vicinity of ℓ'. The imaginary part is only active for $\ell \approx \ell'$ reflecting the presence of strong absorption at the nuclear surface.

The success of the Frahn-Venter parametrization in predicting the experimental values is illustrated for Fraunhofer-type scattering in Fig. 2.4 and for Fresnel-type scattering in Fig. 2.5:

Fig. 2.4. Differential cross-section for elastic scattering of ^{12}C + ^{12}C at E_{lab}=127 MeV. The theoretical curve was obtained with the Frahn-Venter diffraction model.

Fig. 2.5. Differential cross-section ratio to the Rutherford cross-section for the reaction ^{12}C + ^{181}Ta at 122.5 MeV.

II.3 The Rainbow Model
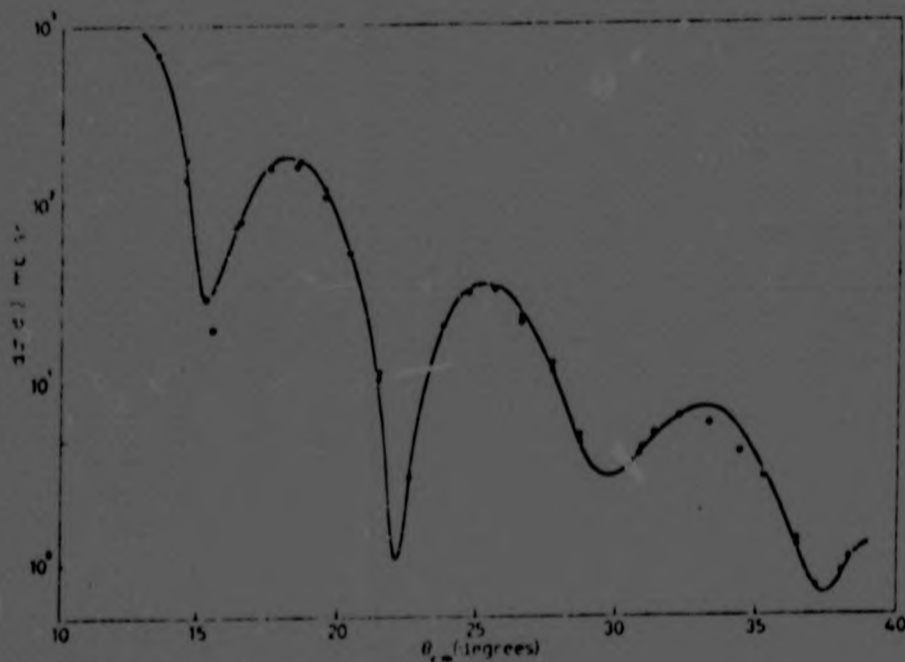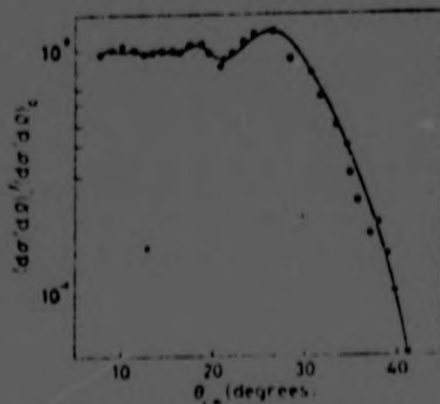
An alternative semiclassical treatment was put forward by Ford and Wheeler [5] and was named the "rainbow model" because of its relation to the scattering of light waves from water droplets. The rainbow model takes as its starting point the relationship for the cross-section

$$\sigma(\theta) = \left| \, \lambda \sum_{\ell=0}^{\infty} (2\ell+1) \, (e^{2i\delta_\ell}-1) \, P_\ell (\cos\theta) \, \right|^2$$

It is a two-parameter, "soft-core" model in which the scattering nucleus is assumed to have a central attractive region and a non-absorptive, refractive surface layer. The rainbow model makes use of a number of approximations.

The phase shift δ_ℓ is replaced by the value calculated in J.W.K.B.L. approximation

$$\delta_\ell = \frac{\pi}{2} \, (\ell+\tfrac{1}{2}) \, -kr_o + \int_{r_o}^{\infty} (k(r)-k) \, dr \tag{2.23}$$

where $k = \frac{2\pi}{\lambda}$, $k(r) = \left[\frac{2m(E-V)}{\hbar^2} - (\ell+\tfrac{1}{2})^2 \frac{1}{r^2} \right]^{\frac{1}{2}}$

and r_o is the turning point of the classical motion defined by $k(r) = o$.

This approximation is valid if $\frac{\lambda}{2\pi V} \frac{dV}{dr} \ll 1$.

The Legendre polynomial is replaced by the asymptotic expression

$$P_\ell(\cos\theta) \sim \frac{2}{\ell\pi\sin\theta} \sin\left[(\ell+\tfrac{1}{2})\theta + \frac{\pi}{4} \right] \tag{2.24}$$

valid for $\theta\ell \gg 1$.

The summation over ℓ is replaced by an integral. This is a valid procedure if many partial waves contribute to the scattering and if the phase shift varies slowly

and smoothly with . The scattering cross-section becomes:

$$\sigma(\theta) = |f(\theta)|^2 = |\frac{1}{k\sqrt{2\pi\sin\theta}} \int_0^\infty d\ell \sqrt{\ell+\tfrac{1}{2}} \left[\exp i\phi+ - \exp i\phi-\right]|^2 \quad (2.25)$$

where $\phi\pm = 2\delta_\ell \pm (\ell+\tfrac{1}{2})\theta \pm \pi/4$

The integrand is a rapidly varying function of ℓ. Only partial waves in the neighbourhood of the point of stationary phase will contribute. Using the saddle-point method the scattering cross-section is given by the formula

$$\sigma(\theta) = \frac{(\ell_\theta+\tfrac{1}{2})\lambda^2}{\sin\theta} \frac{1}{|\frac{\partial\Theta}{\partial\ell}|_{\ell_\theta}} \quad (2.26)$$

where $\Theta_\ell = \frac{2\partial\delta_\ell}{\partial\ell}$ is the classical deflection function

of ℓ where the phase $\phi\pm$ is stationary.

ℓ_θ denotes the value for which $2\frac{\partial\delta_\ell}{\partial\ell} = \pm\theta$

This derivation is not valid near the so-called rainbow angles where the classical deflection function has an extremum (Fig. 2.7):

Fig. 2.6 . Plot of trajectories of ^{16}O nuclei incident on ^{232}Th with $E_{c.m.}$ = 128 MeV.
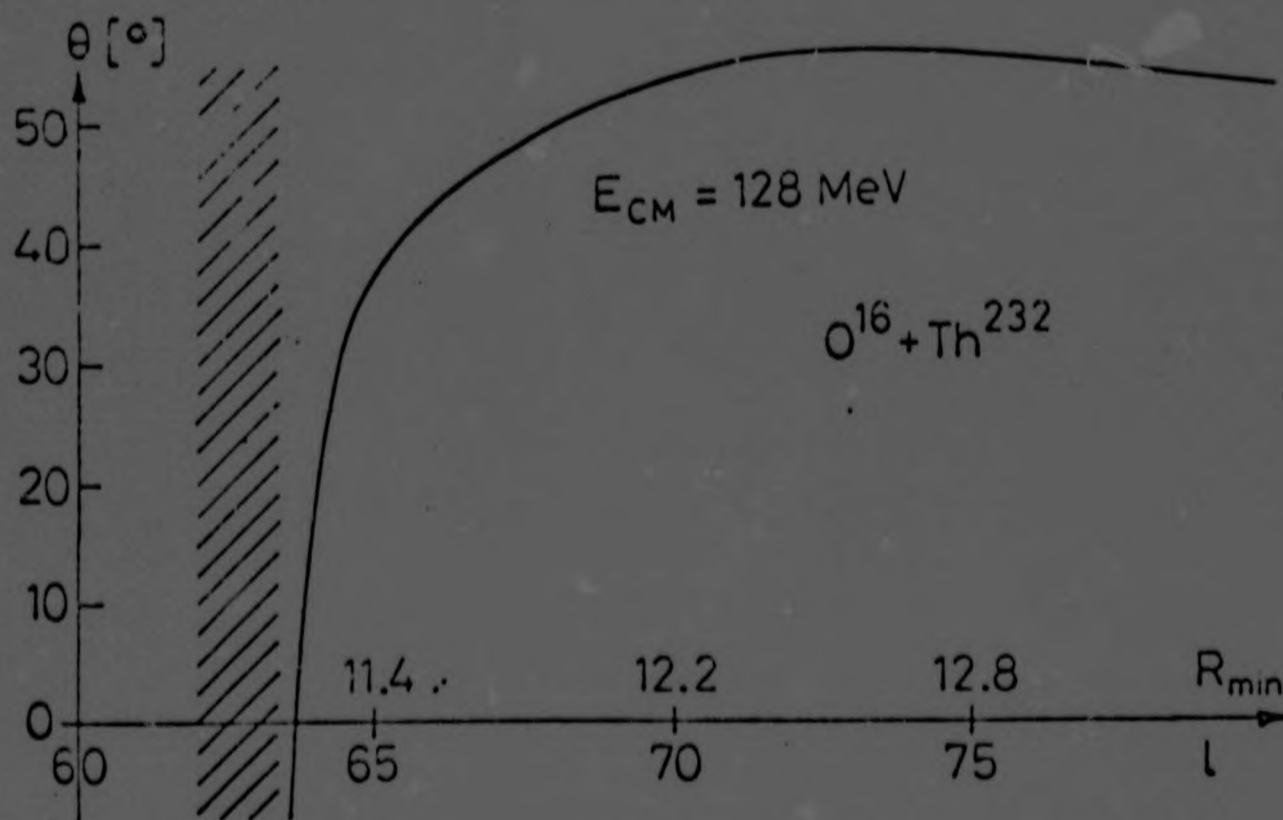

Fig. 2.7. Plot of the classical deflection function against R illustrating the extremum

The effect of large absorption at small angles can be seen in Fig. 2. 6.   For this reason the theory is not expected to be successful for small angle scattering.

At the rainbow angle the deflection function may be expanded in the form

$$\Theta_\ell = \theta_r - q (\ell - \ell_r)^2 \tag{2.27}$$

where θ_r is the value of the deflection function at the extremum.

The variables q and θ_r are the two parameters of the rainbow model.

Now $2 \frac{\partial \delta_\ell}{\partial \ell} = \Theta_\ell$

Therefore this approximation for the deflection function gives the phase shift δ_ℓ as:

$$\delta_\ell = \zeta_r \pm \frac{1}{2} \theta_r (\ell - \ell_r) + \frac{1}{6} q (\ell - \ell_r)^3 \tag{2.28}$$

Substituting this into 2.17 leads to the formula:

$$\frac{\sigma(\theta)}{\sigma_R(\theta)} = \frac{1}{\eta} \frac{2 \sin^2(\theta_r/2)}{q^{2/3}} [Ai(x)]^2 \tag{2.29}$$

where Ai(x) is the Airy integral.

$$Ai(x) = \frac{1}{2\pi} \int exp (ix\mu + \frac{1}{3}i\mu^3) d\mu \tag{2.30}$$

$$\text{and } x = q^{-1/3} (\theta - \theta_r) \tag{2.31}$$

Ai(x) is an oscillating function for $\theta \leq \theta_r$ (bright side) and decreases exponentially for $\theta >> \theta_r$ (dark side).

θ_r can be associated with the interaction radius R through

$$R = \eta \lambda [1 + cosec (\frac{\theta_r}{2})] \tag{2.32}$$

and q can be associated with a non-absorptive surface layer

of thickness ΔR,

$$q = \frac{\theta_r}{(R \Delta R)^2} \tag{2.33}$$

A typical fit of the model to the data is shown for 27.3 MeV ^{14}N scattered on ^{27}Al where θ_r and q have been set at $\theta_r = 94°$ and q=0.30 corresponding to $r_0 = 1.59$ fm and $\Delta R = 0.83$ fm:
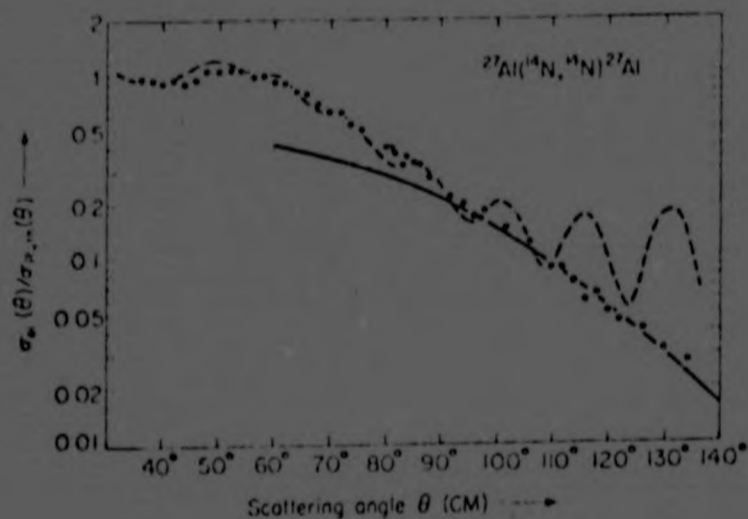
Fig. 2.8. Angular distribution of elastically scattered 27.3-MeV^{14}N ions on ^{27}Al, the experimental data being compared with the predictions of Blair sharp cut-off theory (dashed curve) and rainbow scattering theory with $\theta_r = 94°$ and q=0.30 (solid curve).

We have seen that the semiclassical diffraction models are able to predict results having fairly good agreement with experiment. However the parametrization which is made in these models does not lead to a deeper understanding of the underlying many-body problem. One may hope to achieve a better insight by studying an interaction potential.

CHAPTER III

The Optical Model

III.1 Introduction

The usefulness of the optical model for heavy-ion
scattering was appreciated from the early days of work in
this field [6].   It is well known that the optical model
associates the partial transmission and partial absorption
of particles incident upon a nucleus with the real and
imaginary parts of a complex potential in analogy with
the propagation of light by a refractive medium in optics.
That is, the nuclear potential takes the form:

$$V_{nucl}(r) = U(r) + i\, W(r) \tag{3.1}$$

Since the optical model provides a method for
predicting variations in the cross-section for elastic-
scattering it is hoped that by varying parameters which are
known to change from system to system one could account
for the different cross-sections observed for different
systems.   Information about the structure of the nucleus
can then hopefully be extracted by relating these parameter
variations to differences in the nuclear structure and the
reaction mechanism.

There are a variety of ways to specify the radial
dependance of the optical potential.   Observing that the
nuclear mass densities may be well approximated by Woods-
Saxon shapes and that the nuclear forces are short ranged
and saturating, one may assume a Woods-Saxon form for the

real part of the potential and a derivative of the Woods-Saxon form or Gaussian form for the imaginary part of the potential. This approach allows for the occurrence of surface absorption.   One then has

$$V_{nucl}(r) = U_o \frac{1}{1+\exp(\frac{r-R}{a})} +iW_o \frac{d}{dr} \frac{1}{1+\exp(\frac{r-R'}{a'})}$$

$$\text{or}\quad V_{nucl}(r) = U_o \frac{1}{1+\exp(\frac{r-R}{a})} +iW_o \frac{1}{\exp(\frac{r-Ro}{b})^2} \tag{3.2}$$

An even more extensively used approach is to assume a Woods-Saxon form for both real and imaginary parts, which corresponds to volume absorption.

$$V_{nucl}(r) = U_o \frac{1}{1+\exp(\frac{r-R}{a})} + iW_o \frac{1}{1+\exp(\frac{r-R'}{a'})} \tag{3.3}$$

In most heavy-ion analyses to date a simple four-parameter complex potential of the Woods-Saxon form has been used where the real and imaginary parts are considered to possess the same geometry.

$$V_{nucl}(r) = (U_o+iW_o) \frac{1}{1+\exp(\frac{r-R}{a})} \tag{3.4}$$

III.2 Woods-Saxon fits

The Yale group have provided optical model fits for a number of identical nuclei scattering processes [7].   In their earliest fits [8] they chose parameters which were close to the known values of nuclear radii and surface diffusities.   Thus for $^{16}O-^{16}O$ scattering the parameters that were used were:

Uo[MeV]	R[fm]	a[fm]	Wo[MeV]	R'[fm]	a'[fm]
17.0	6.8	0.49	0.4+0.1Ec.m.	6.8	0.49

The total nucleus-nucleus potential has nuclear, Coulomb and angular momentum contributions. Using the above parametrization of the nuclear contribution we can represent the radial dependance of the effective potential as shown in Fig. 3.1:

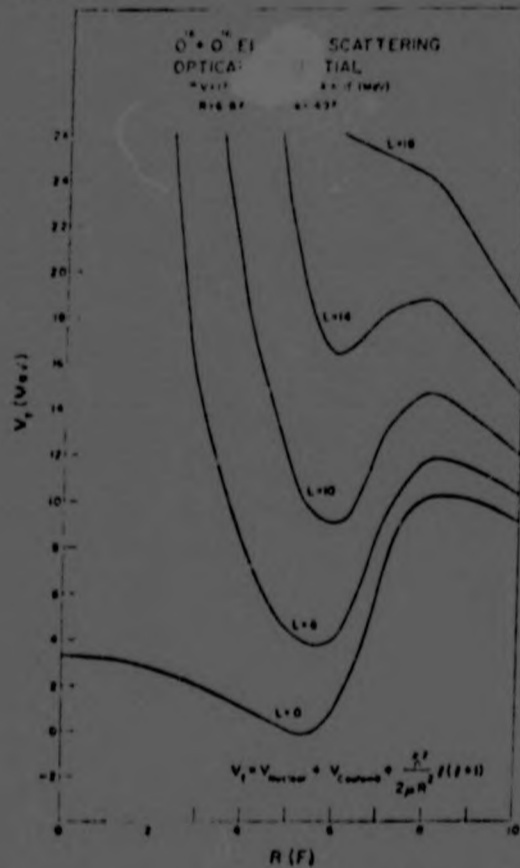Fig. 3.1. Radial dependence of the real part of the optical potential for several partial waves.

The elastic-scattering excitation functions predicted by this parametrization of Maher et al. is compared to the experimentally observed values in Fig 3.2:
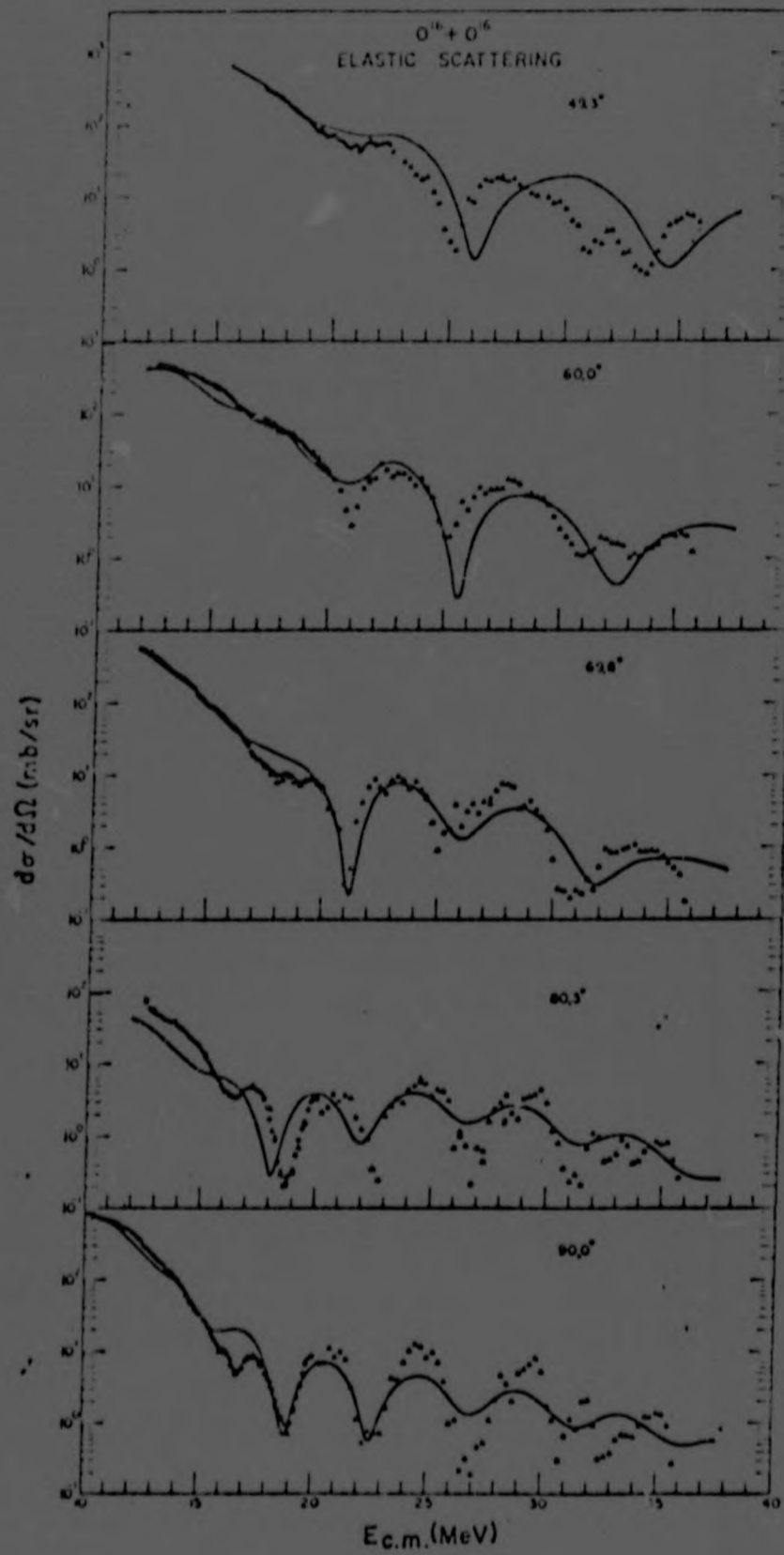
Fig. 3.2. $^{16}O-^{16}O$ elastic scattering excitation functions. The solid line represents the cross-sections calculated with the optical potential of Maher et al [1].

The early parametrization was unable to reproduce the
large oscillations found in the ^{16}O-^{16}O excitation function.
The diffraction model indicates that the amplitude of the
oscillation in the excitation function will increase with
decreasing diffuseness parameter. An improved fit was
then made using the following parameters -

Uo[MeV]	R[fm]	a[fm]	Wo[MeV]	R'[fm]	a'[fm]
17.0	6.8	0.49	0.8+0.2Ecm.	6.4	0.15

The new value of a' no longer bears a relation to the
physical structure of the nucleus. It is possible however
to account for this requirement by incorporating an
angular momentum dependance in the imaginary potential.

III.3 Angular momentum dependant potentials

The absorptive part of the potential in the optical
models we have so far considered have been independant of
angular momentum. The necessity for introducing an
angular momentum dependance in the optical potential can
be appreciated by considering the dependance of the optical
model on conserved quantum numbers.

In the scattering of two complex nuclei, it is in
general not a valid assumption to assume that each partial
wave is attenuated at the same rate as any other wave once
it enters the absorptive region, since one expects the
amount of absorption for a given partial wave to reflect
the density of states in the compound system at that
energy and angular momentum. From a consideration of
conserved quantum numbers, Chatwin et al [9] were able to
modify the form of the optical potential to include

a smooth cut-off in the strength of the absorptive potential with increasing angular momentum.

Further evidence for the desirability of having an angular momentum dependance in the imaginary potential is presented by the improved fit found by the Yale group for the scattering of ^{16}O on ^{16}O. They found that it was necessary to reduce the diffuseness parameter to a physically unreasonable size to give an improved fit. Such a variation in coordinate space is equivalent to having an angular momentum dependance in angular momentum space.

A qualitative justification for an angular momentum dependance can be outlined within a modified Feshbach formalism of reaction theory [10].

Defining P_c to be the projection operator giving elastic scattering into channel c and $Q_c = 1 - P_c$ to be the non-elastic operator, we have in perturbation theory the following expression for the optical operator:

$$H_c^{opt}(E) = P_c H P_c - \sum_n \frac{P_c H Q_c |n\rangle \langle n| Q_c H P_c}{E_n - E}$$

$$+ \wp \int_{E_a'}^{\infty} \frac{W_o^{opt}(E')dE'}{E' - E} + iW_o^{opt}(E) \qquad (3.5)$$

where H is the total Hamiltonian for the system and the absorption operator is

$$W_c^{opt}(E) = -\pi \sum P_c H Q_c |\nu, E\rangle \langle \nu, E| Q_c H P_c$$

$$E > E_a'$$

$$= 0 \qquad E \leq E_a' \qquad (3.6)$$

$\wp$ denotes the Cauchy principal value.

The states $|n\rangle$ and $|\nu, E\rangle$ are bound and continuum

eigenstates of the operator $Q_c H Q_c$ with eigenvalues E_n and E' respectively.

The operator H_c^{opt} is diagonal in total angular momentum and parity. Since $P_c H Q_c$ conserves angular momentum L and parity π, the elastic-scattering channel with a given value of ℓ^π couples only to those states $|n\rangle$, $|v,E'\rangle$ which have the same value of ℓ^π so that in general H_c^{opt} is ℓ^π dependant.

Now by their construction the states $|v,E\rangle$ have no incident-channel contributions. Also the operators $P_c H Q_c$ and $Q_c H P_c$ are rotationally invariant and therefore the degree of overlap between the states $|v,E\rangle$ and these operators is a function of the non-elastic angular momentum

$$\underset{\sim}{\ell'} = \underset{\sim}{j'} + \underset{\sim}{i'_1} + \underset{\sim}{i'_2} \tag{3.7}$$

that can be carried away in the final states. $\underset{\sim}{i'_1}$ and $\underset{\sim}{i'_2}$ are the final spins of the fragment nuclei which are generally small. So with increasing ℓ an increasing amount of angular momentum, $\underset{\sim}{j'}$, must be carried away in the relative motion of the fragments. However the repulsive centrifugal barrier also grows with ℓ. Since $P_c H Q_c$ is a short-ranged operator, the overlap with $|v,E,\ell^\pi\rangle$ will become smaller. Consequently, the strength of the optical operator corresponding to absorption should decrease as ℓ exceeds a certain value ℓ_c which is characteristic of the non-elastic channels.

In order to achieve a calculational form of the theory a conventional optical potential is employed and a smooth

but rapid angular momentum cut-off of the absorption
potential strength is included. To describe the
situation that the incident nucleus can carry in more
angular momentum than can be carried away in any of the
reaction channels the model must show that for these
angular momentum values the elastic wave will not be
attenuated even in the nuclear interior, reflecting the
poor matching of the elastic and reaction channels. The
absorption is therefore given the following ℓ-dependance:

$$W(r,\ell) = W_o \; \frac{1}{1+\exp(\frac{\ell-\ell_c}{\Delta\ell})} \; \frac{1}{1+\exp(\frac{r-R}{a})} \tag{3.8}$$

where ℓ_c is an average characteristic cut-off in angular
momentum for the non-elastic channels and $\Delta\ell$ is the region
over which the cut-off takes place.

In general the cut-off ℓ_c is a function of energy
because the maximum angular momentum increases as energy
increases. A classical argument can be made which
produces the following relationship:

$$\ell_c = k_c(E)R_c \tag{3.9}$$

where $k_c(E)$ represents an average wave number for the
non-elastic channels, and R_c reflects the average size of
the interacting system.

It has been possible [11] to understand some properties
of the angular momentum dependant potential in terms of
the strong absorption model. If the reflection coefficients
calculated with an angular momentum independant imaginary
potential are denoted by $\eta_o(\ell)$ and those obtained by

including the smooth cut-off are denoted by μ_ℓ, the
following relation is derived:

$$|\eta_\ell| = |\eta_o(\ell)|^{f(\ell)} \qquad (3.10)$$

where $f(\ell)$ is the angular momentum dependance of the
imaginary potential given by $f(\ell) = \dfrac{1}{1+\exp(\frac{\ell-\ell_c}{\Delta \ell})}$ $\qquad$ (3.11)

This equation implies that for values of ℓ_c which are
large compared to the grazing angular momentum ℓ_o the ℓ
cut-off will have no effect since $f(\ell)=1$ for those ℓ values
for which the nuclear phase shift is different from zero,
i.e. $|\eta_\ell| = |\eta_o(\ell)|$ for $\ell_c >> \ell_o$. ℓ_o is defined by $|\eta_o(\ell_o)|=\frac{1}{2}$.

On the other hand very small values of ℓ_c may be
excluded since this gives a potential that is transparent
for low partial waves which are strongly absorbed.

An angular momentum cut-off effect will only be
observed for values of ℓ_c not too different from the
grazing angular momentum.   This limits the value of ℓ_c
to values around ℓ_o.

The standard optical model potential is not adequate
to explain the elastic scattering for very strongly bound
nuclei such as ^{16}O-^{16}O and ^{16}O-^{40}Ca since these are not
easily excited.   However the extension of the optical
model to include an angular momentum dependant absorption
term is able to give a better description of the data.

A fit of an optical potential having an angular
momentum dependant imaginary part for the ^{16}O-^{16}O interaction
is seen to give excellent agreement up to a centre of mass
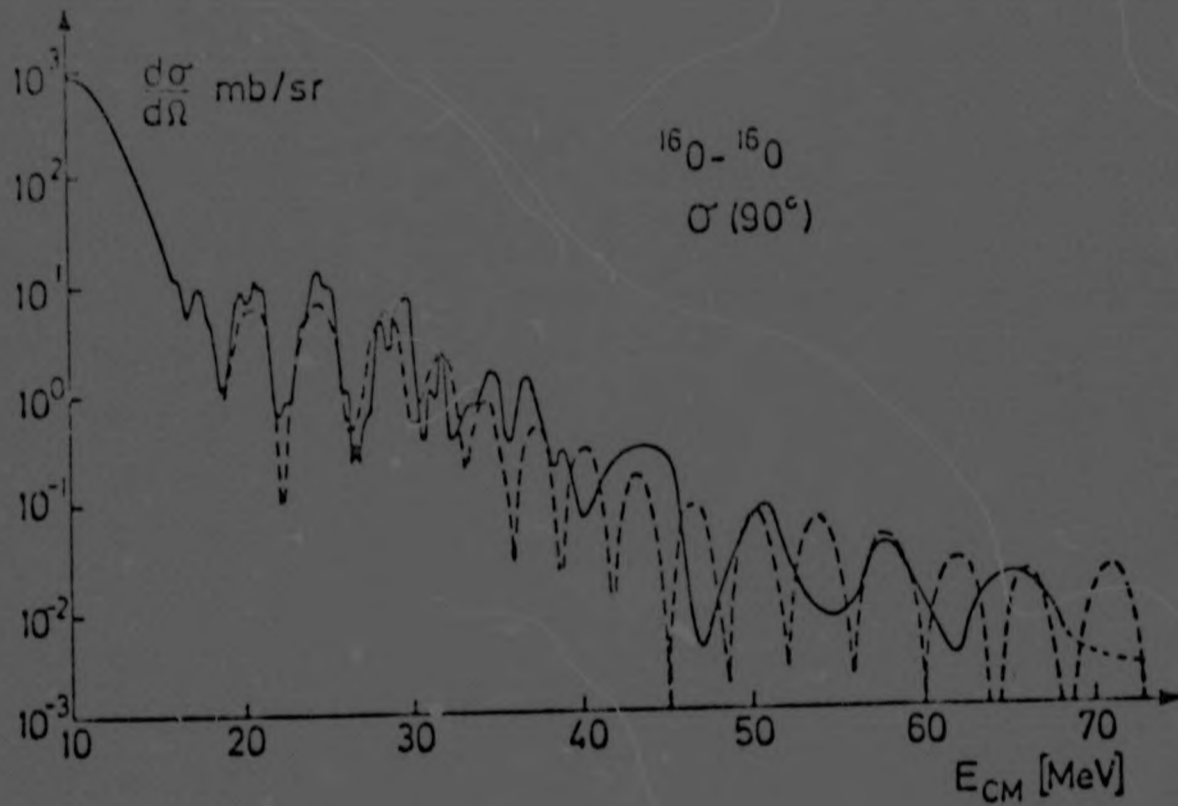energy of about 35 MeV (Fig. 3.3) :

Fig. 3.3. In the high energy region the excitation function calculated with a ℓ-dependent absorption (dashed line) oscillates too fast in comparison with the experimental curve.

However above 35 MeV the predicted cross-section is seen to have oscillations which vary more rapidly than those observed for the experimental cross-section.

CHAPTER IV

The Extended Liquid Drop Model

IV.1 Introduction

The Thomas-Fermi approximation [12], a statistical
theory, has proved to be easier to handle than the
Hartree-Fock method in the investigation of nuclear structure.
Following the success enjoyed by the statistical theory in
treating nuclear-surface effects [13], the theory was
applied to finite nuclei [14]. By making assumptions on
the energy density and then expressing the total energy of
the many nucleon system as a functional, $E[\rho]$, of the local
density, $\rho(r)$, it is possible to find the ground-state
density distribution by minimization of $E[\rho]$ with respect
to $\rho(r)$. The need for a more fundamental description of
the heavy-ion interaction led to the statistical approach
being extended [15] to derive the potentials present in
heavy-ion collisions.

IV.2 The Energy Functional

For a complete treatment of a collision of finite
nuclei a knowledge of the nuclear two-body force as well
as a method for treating the many-body problem is
necessary. However for such a treatment it is necessary
to calculate the self-consistent average potential

$$U(m) = \sum_{n<k_F} \langle mn|V|mn \rangle \qquad (4.1)$$

which is at present not possible for the heavy-ion
scattering problem.

For infinite nuclear matter however the problem is
much simplified as translational invariance exists and the
Coulomb energy is absent. This gives rise to state
vectors which are plane waves and the self-consistency
problem reduces to the definition of the single-particle
energies

$$E_p = \frac{h^2}{2m} + U(p) \qquad (4.2)$$

We would therefore like to make extensive use of
infinite nuclear matter results for the description of
finite nuclei. The Thomas-Fermi approximation proves to
be a suitable framework in which to exploit these results.
It has been shown [16] that for a quantum-mechanical system
the energy can be expressed as a unique functional of the
density. As this functional is complicated and unknown
we attempt, by application of the statistical theory, to
approximate it in some semiclassical fashion.

For slowly varying densities, an expansion of the
energy in powers of the density gradient can be made.
Since the shell structure can be considered to arise from
the quantum oscillations created by the vanishing of the
density outside the nucleus, such a procedure would lose
this structure. The Thomas-Fermi approximation consists
in assuming that the energy dependance in the density is
locally the same as that of a homogeneous medium in the
ground state. This is equivalent to assuming that the

correlations between the nucleons in finite nuclei are the
same as between nucleons in infinite nuclear matter and is
known as the local density approximation. When the
density is low, the de Broglie wavelength associated with
each nucleon becomes relatively large and this theory breaks
down. We now investigate the energy functional that must
be minimized.

It has been pointed out that the energy functional is
a complicated and unknown function of the density. It has
therefore become the practice[12][14][15] to assume some kind
of reasonable schematic expression to represent this
functional dependance. The approach we consider is that
proposed by Scheid and Greiner in Ref(15). This approach
allows the nuclear density to be found as the solution of
linear differential equations.

They consider the dependance of the binding energy
$E[\rho]$ of a nucleus consisting of A nucleons and Z protons
on the nuclear density distribution ρ.

$$E[\rho] = W_0 A + \frac{C}{2\rho_0} \int (\rho - \rho_0)^2 \, d\tau + \sum_{i=1}^{2} \frac{V_i}{8\pi} \int \int \rho(r_1) \frac{e^{-|r_1 - r_2|/\mu_i}}{|r_1 - r_2|} (\rho(r_2) - \rho(r_1)) \, d\tau_1 \, d\tau_2$$

$$+ \frac{1}{2}\left(\frac{eZ}{A}\right)^2 \int\int \frac{\rho(r_1)\rho(r_2)}{|r_1 - r_2|} \, d\tau_1 \, d\tau_2 + \frac{G}{2\rho_0}\left(\frac{2Z}{A}-1\right)^2 \int \rho^2 \, d\tau \qquad (4.3)$$

The first term is an energy proportional to the number
of nucleons. The second term allows for the effect of
compression and is essentially repulsive. The next term
describes two interactions of Yukawa type with ranges μ_i and
potential strengths V_i. Two interactions are included for

completeness as it is only necessary to have a single
interaction of Yukawa type to reproduce the elastic-
scattering cross-section quite well. The fourth term in
expression 4.3 is the classical Coulomb energy. The final
term is included to describe symmetry effects. If
different proton and neutron densities are present they
can be allowed for by replacing the final term by
$\frac{G}{2\rho_0} \int (\rho_P - \rho_N)^2 \, d\tau$, where ρ_P and ρ_N are the proton and
neutron density distributions respectively.

Making use of same physical constraints one is able
to derive a set of differential equations from the
expression (4.3). One requires constant particle
number A, i.e.

$$A = \int \rho \, d\tau \tag{4.4}$$

and that the nucleus has a surface at r=R, i.e.

$$\rho(R) \, 4\pi R^2 \, \delta R + \int_o^R \delta\rho \, d\tau = o \tag{4.5}$$

The Yukawa and Coulomb potentials ψ_i and ϕ are given by

$$\psi_i(r) = \frac{V_i}{4\pi} \int \frac{e^{-|r-r'|/\mu_i}}{|r-r'|} \rho(r') \, d\tau' \tag{4.6}$$

and $\quad \phi(r) = \frac{eZ}{A} \int \frac{1}{|r-r'|} \rho(r') \, d\tau' \tag{4.7}$

The Yukawa potential satisfies :

$$\nabla^2 \psi_i - \frac{1}{\mu_i^2} \psi_i = -V_i \rho \tag{4.8}$$

and the Coulomb potential satisfies:

$$\nabla^2 \phi = -4\pi \frac{eZ}{A} \rho \tag{4.9}$$

Rearranging, equation 4.3 becomes:

$$E[\rho] = (W_o - C)A + \frac{C}{2\rho_o} \int \left(\frac{1}{V^2} \rho^2 + \rho_o^2 \right) d\tau + \frac{1}{2} \int \rho(\psi_1 + \psi_2) \, d\tau$$

$$+ \frac{eZ}{2A} \int \rho\phi \, d\tau \qquad (4.10)$$

where $\qquad \frac{1}{V^2} = 1 - (V_1\mu_1^2 + V_2\mu_2^2)\frac{\rho_o}{C} + \left(\frac{2Z}{A} - 1\right)^2 \frac{G}{C} \qquad (4.11)$

One varies the binding energy with respect to the density. Assuming a surface at r=R, we obtain:

$$\delta E = \int \left(\frac{C}{\rho_o V^2} \rho + \psi_1 + \psi_2 + \frac{eZ}{A}\phi \right) \delta\rho d\tau$$

$$+ \left(\frac{C}{\rho_o V^2} \rho(R) + \psi_1(R) + \psi_2(R) + \frac{eZ}{A}\phi(R) \right) \rho(R) 4\pi R^2 \delta R$$

$$+ \frac{C}{2\rho_o} \left(\rho_o^2 - \frac{1}{V^2}\rho^2(R) \right) 4\pi R^2 \, \delta R \qquad (4.12)$$

Equation 4.5 gives us $\rho(R) \, 4\pi R^2 \delta R = -\int \delta\rho d\tau$

Substituting this in 4.10 and imposing the condition $\delta E=0$ requires that :

$$\frac{C}{\rho_o V^2} \rho + \psi_1 + \psi_2 + \frac{eZ}{A}\phi = \text{const} \qquad (4.13)$$

and $\qquad \rho(R) = V\rho_o \qquad (4.14)$

The system of equations has a unique solution for a stable equilibrium density. In the absence of Coulomb, symmetry and Yukawa forces the density distribution is found to be of square well shape with constant value $\rho = \rho_o$. The Yukawa force causes surface effects leading to a decrease in the density in the nuclear surface if the force is attractive.

It is possible to postulate a general solution to these equations. It has the form

$$\rho = \sum_{i=1}^{3} a_i \, j_o(a_i r) \tag{4.15}$$

where j_o is the spherical Bessel function.

A useful aid in solving these equations is the integral:

$$\frac{1}{4\pi} \int_{o}^{R} \frac{e^{-|\underline{r}-\underline{r}'|/\mu}}{|\underline{r}-\underline{r}'|} \, j_o(ar') \, d\tau'$$

$$= \frac{1}{\mu^{-2}+a^2} \left\{ j_o(ar) - e^{-R/\mu}(\cos \alpha R + \frac{1}{\mu a} \sin \alpha R) \, j_o(\frac{ir}{\mu}) \right\} \tag{4.16}$$

Making use of the fact that this integral provides the homogeneous and the inhomogeneous solutions to equation 4.8 and that the sum of the inhomogeneous solutions must separately vanish, fixes the parameters a_i as the roots of an equation cubic in a_i^2.

$$\frac{C}{\rho_o v^2} + \frac{V_1}{\mu_1^{-2}+a_i^2} + \frac{V_2}{\mu_2^{-2}+a_i^2} + 4\pi(\frac{eZ}{A})^2 \frac{1}{a_i^2} = 0 \tag{4.17}$$

Demanding that the sum of the inhomogeneous solutions of the two Yukawa potentials also vanish gives two relations for the a_i.

$$\sum_{i=1}^{3} a_i \frac{1}{\mu_k^{-2}+a^2} \quad \cos \alpha R + \frac{1}{\mu_k \alpha} \sin \alpha R = 0 \quad k=1,2 \tag{4.18}$$

A third condition arises from the boundary condition 4.14.

$$\sum_{i=1}^{3} a_i \, j_o(a_i R) = v\rho_o \tag{4.19}$$

It is now possible to express the a_i as a function of the nuclear radius R and thus obtain the equation

$$A = 4\pi R^3 \sum_{i=1}^{3} \frac{a_i j_1(a_i R)}{a_i R} \tag{4.20}$$

Equation 4.20 can be solved by an iterative method.

IV.3 The parameters in the theory

We now consider how the constants W_o, C, ρ_o, V_1, V_2, μ and G are determined. We restrict ourselves to the presence of only one attractive Yukawa force having parameter V.

The value of G is determined by requiring the proper ratio of $\frac{Z}{A}$ for the variation of binding energy with respect to $\frac{Z}{A}$. W_o, ρ_o and V can be fixed by three experimental values; namely the mean square radius of one arbitrary nucleus and the binding energies of two other arbitrary nuclei. The only two remaining parameters C and μ are determined by observing what values of these parameters give the best fit to the elastic-scattering cross-section data. Thus the data of two nuclei fix all the parameters.

The dependance of the results on the choice of the parameters C and μ can be seen for the case of $^{16}O-^{16}O$ scattering by choosing two different sets of values for C and μ.

The first choice is $C = \frac{100}{9}$ MeV and $\mu = 0.8$ fm.
This leads to the following values for the other parameters:

$W_o = -16.0$ Mev $\rho_o = 0.188$ fm^{-3}

$V = -469$ MeV fm $G = 70$ MeV   (4.21)

The second choice is $C = \frac{80}{9}$ MeV and $\mu = 0.3$ fm.
This leads to the following values for the other parameters:

$W_o = -15.3$ MeV . $\rho_o = 0.176$ fm^{-3}

$V = -13012$ MeV fm $G = 70$ MeV   (4.22)

These parameters determine the behaviour of various nuclear quantities. From equation 4.3 it can easily be seen that disregarding Coulomb and symmetry energies the binding energy of a nucleon in infinitely extended nuclear matter is given by :

$$\frac{E}{A} = W_o + \tfrac{1}{2} C \frac{\rho_o}{\rho} (\frac{\rho}{\rho_o} -1)^2 \qquad (4.23)$$

It is thus possible to plot the variation of binding energy of nuclear matter with nuclear density according to equation 4.23. This plot is shown in Fig.4.1 and is compared to the saturation curve obtained in the Brueckner theory of nuclear matter.
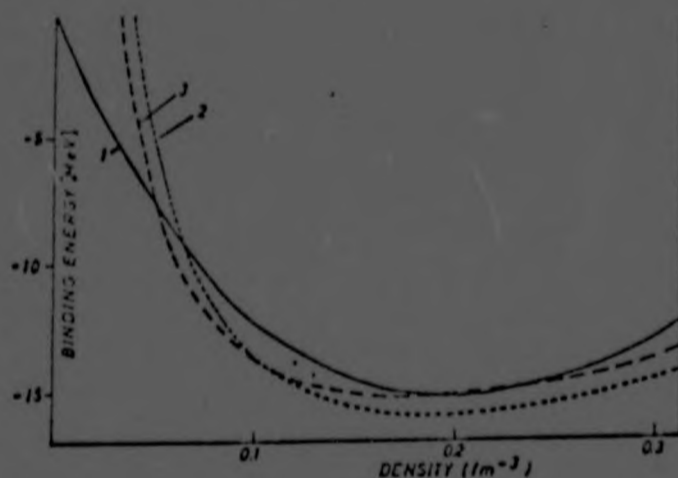

Fig. 4.1. The binding energy per nucleon in infinite nuclear matter with an equal number of protons and neutrons and without Coulomb energy. The solid line represents Brueckner's results. Curves 2 and 3 (dotted) are calculated with the parameter sets 4.21 and 4.22 respectively.

It is also possible to plot the binding energy per nucleon, the proton number Z, the constant of the surface thickness Y, the equivalent radius R_{eq} and the surface thickness t as functions of the nucleon number A. This is done in Figs. 4.2 and 4.3 for the two sets of parameters 4.21 and 4.22. The radial density distribution for two different nuclei is also shown.
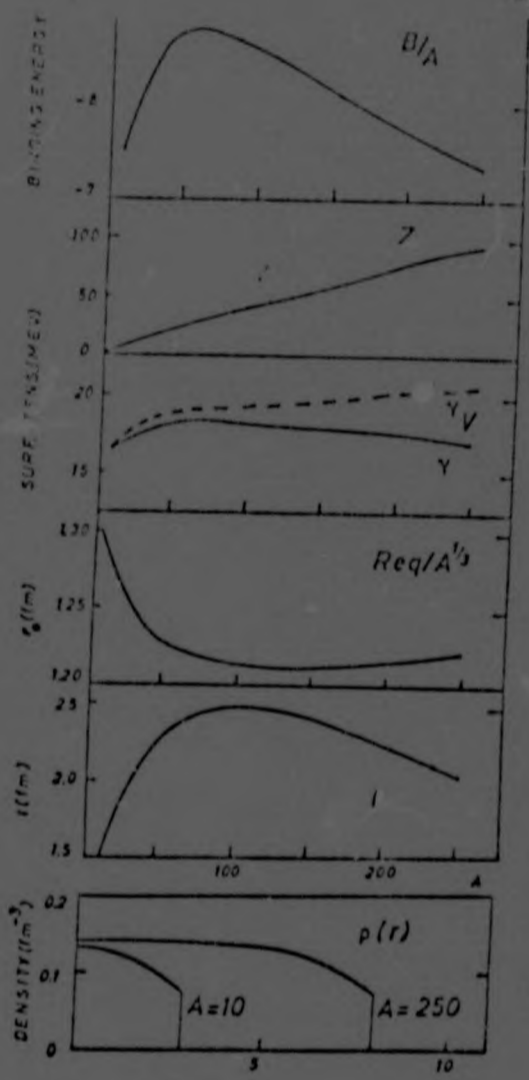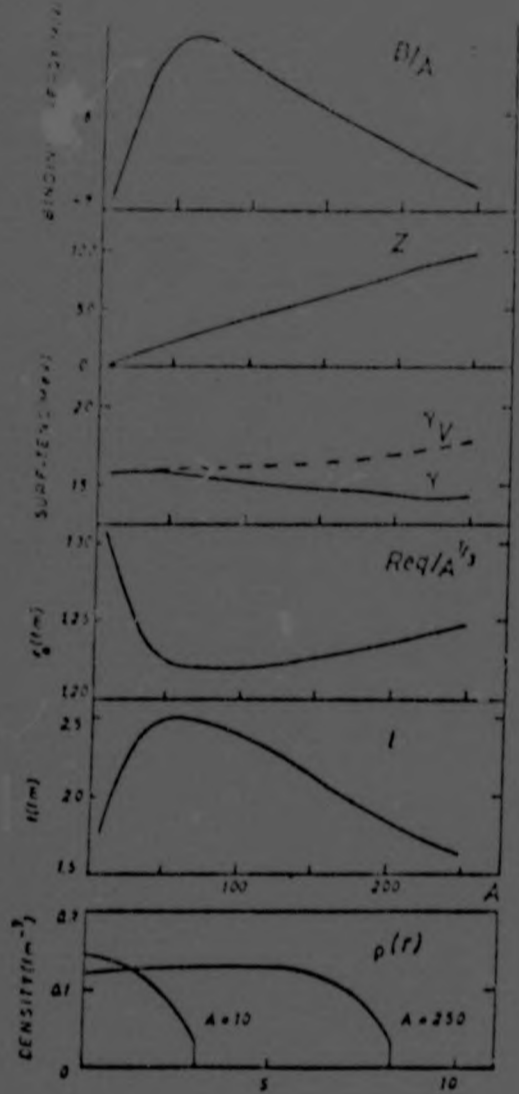
Fig. 4.2. The binding energy per nucleon, the proton number Z, the co... ant of the surface tension γ, the equivalent radius R_eq and the surface thickness t as functions of the nucleon number A. In addition the radial density distribution for two different nuclei A = 10 and A = 250 are shown for parameter set 4.21.

Fig. 4.3 The same quantities as in Fig. 4.2, but for parameter set 4.22.

IV. 4 The Real Part of the Potential

We will now consider how the above theory can be applied to derive the real part of the optical potential for ion-ion collisions.   We consider the particular case of $^{16}O-^{16}O$ scattering.   As the nuclei begin to interpenetrate distinct processes may occur.   There are two extreme possibilities.   In the one, compression of nuclear matter

the two phase, whereas in the other, compression of nuclear matter is forbidden. These are known as the sudden and adiabatic approximations respectively.

The energy expression, equation 4.3, and the resulting density for the ^{16}O nuclei is used to give the real part, V(r), of the potential since :

$$V(r) = E\left[\rho \text{ compound system}\right] - 2E\left[\rho \text{ }^{16}\text{O system}\right] \qquad (4.24)$$

where $E\left[\rho \text{ }^{16}\text{O system}\right]$ is the binding energy of the ^{16}O nucleus.

The density of the compound system is given in sudden approximation by:

$$\rho_{c.s.} = \rho_{^{16}\text{O}}(r_1) + \rho_{^{16}\text{O}}(r_2)$$

The meaning of r_1, r_2 and r are made clearer in Fig. 4.4 :
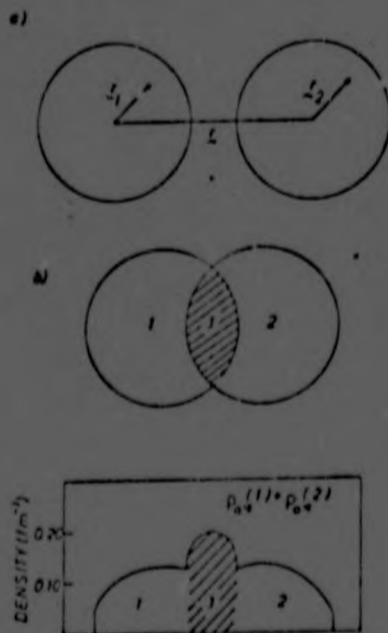

Fig. 4.4. The superposition of the densities: (a) The coordinates r_1 and r_2 are measured from the centres of the nuclei. The coordinate r denotes the relative distance of the two centres. (b) The density distributions of nuclei 1 and 2 overlap in the region 3 shown by the shadowed area, in which the matter is compressed. The lower diagram contains the density distribution along an intercept through the centres of the ^{16}O nuclei.

The density of the nucleus-nucleus system is shown as a function of the separation distance, assuming the sudden approximation, in Fig. 4.5:
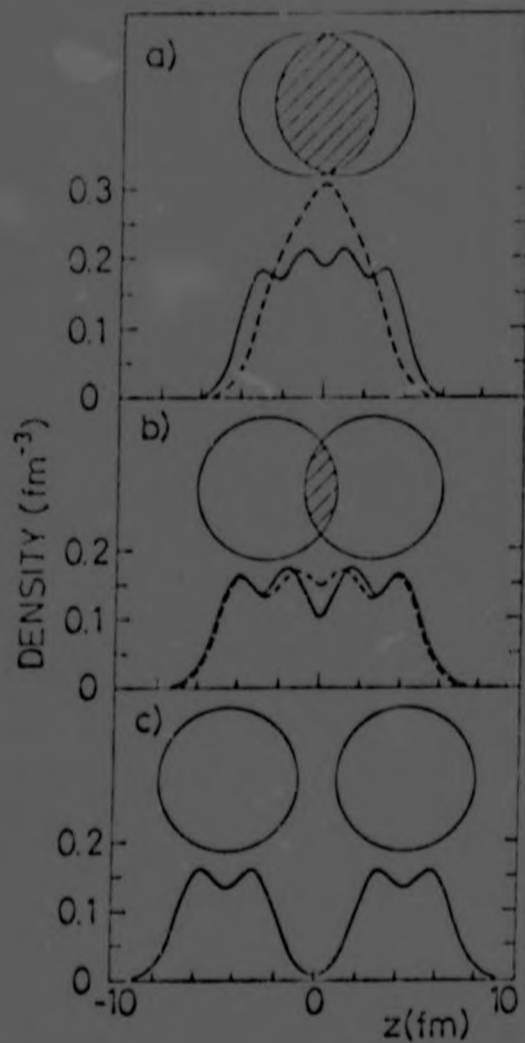

Fig. 4.5. The density of the nucleus-nucleus system in a sudden nucleus-nucleus collision for various distances between the two nuclei.

All integrals appearing in equation 4.24 can be solved analytically for the density distribution given by equation 4.15. The basic integral that appears has the form

$$I(r,\alpha,\beta,\mu) = \frac{1}{4\pi} \int_0^R \int j_0(\alpha r_1) \frac{e^{-|r_1 - r_2 - r|/\mu}}{|r_1 - r_2 - r|} j_0(\beta r_2) \, d\tau_1 d\tau_2 \quad (4.25)$$

Expressing all integrals appearing in 4.24 in terms of
this basic integral reduces 4.24 to:

$$V(r) = \sum_{i,j=1}^{3} a_i a_j \{ \frac{C}{\rho_o v^2} (\frac{1}{\mu^2} I (r,\alpha_i,\alpha_j,\mu))_{\mu \to o}$$

$$+ \sum_{k=1}^{2} V_k I(r,\alpha_i,\alpha_j,\mu_k) + {}^{4\pi}(\frac{eZ}{A})^2 I(r,\alpha_i,\alpha_j,\mu \to \infty) \}$$

$$-\frac{2\pi}{3} R^3 \rho_c C(1-\frac{r}{2R})^2 (1+\frac{r}{4R}) \Theta (1-\frac{r}{2R}) \qquad (4.26)$$

where $\Theta(x)$ is the step function defined by :

$$\Theta(x) = 1 \qquad x>0$$
$$= 0 \qquad x<0$$

If there is no overlapping of the nuclei, only the
Coulomb interaction is effective. The Coulomb barrier is
lowered by the attractive Yukawa force. As the degree of
overlap increases, the presence of repulsive forces becomes
more and more marked and there is a rapid increase in the
potential. Furthermore the density in the overlap region
is highly compressed.

It is also possible to derive the shape of the
potential in the adiabatic approximation. This is
achieved by requiring that matter is nowhere compressed.
The important difference between the potentials derived in
adiabatic and sudden approximation is that no hard core
is present for the adiabatic potential. This results from
forbidding compression effects. The potentials in adiabatic
and sudden approximation, with centrifugal potential added,
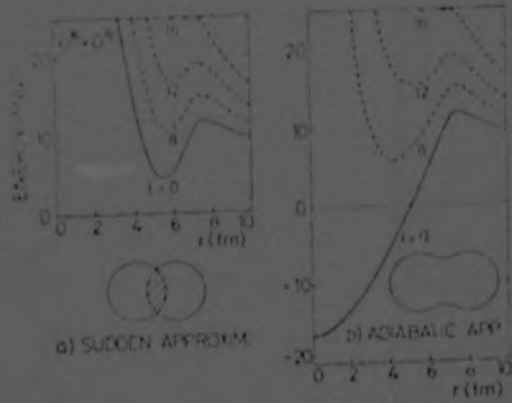are compared in Fig. 4.6 :

Fig. 4.6. Comparison of sudden and adiabatic O^{16}-O^{16} potentials. The centrifugal potential has been added for the various partial waves.

The Two-centre Shell Model

V.1 Introduction

The shell model has been extensively applied to
problems in nuclear physics.   In particular many attempts
have been made to interpret fission phenomena by the use of
a shell model modified to allow for a deformation degree
of freedom.   However in nuclear fission, where the nucleus
splits to form two separate nuclei, it becomes evident that
a model which provides for more than one centre of force
would be more appropriate.   Such a model, the two-centre
shell model, was initially developed[17] to cope with the
phenomenon of nuclear fission and was found to be
successful in overcoming difficulties which had arisen
from applying the deformed shell model to the fission
problem.

The difficulties in applying the deformed shell model
arise from the fact that the sum of single-particle energies
diverges to infinity for large deformations.   This in
turn comes about because the single-particle energies have
a surface energy term and the surface of the deformed
shell model goes to infinity for large deformations.
However the surface in the two-centre shell model does
not diverge for large separations of the centres and thus
the major problem of the deformed shell model does not
arise.   Because of its suitability in this respect and

since this model leads to a molecular type structure for
the fissioning nucleus the application was extended [18]
to the investigation of α-ion potentials in heavy-ion
scattering.

V.2 The Model

The Hamiltonian of the two-centre shell model is
given in cylindrical coordinates by:

$$H = \frac{\hbar^2}{2m} \nabla^2 + U(\underline{p},\underline{s}) + V(Z,\rho) \tag{5.1}$$

In this treatment we will consider the potential of
each centre to have the form of a simple harmonic oscillator
as these can be handled mathematically. The wave functions
can be arrived at analytically and can serve as a basis
for improvement of the model.

$V(Z,\rho)$ is then given by:

$$V(Z,\rho) = \begin{array}{ll} \frac{m}{2}\, \omega_{Z_1}^2\, (Z-Zo_1) + \omega_{\rho_1}^2\rho^2 & Z>0 \\[2mm] \frac{m}{2}\, \omega_{Z_2}^2\, (Z+Zc_2) + \omega_{\rho_2}^2\rho^2 & Z<0 \end{array} \tag{5.2}$$

where Zo_1, Zo_2 is the distance from the origin of the two
centres. ω_{Z_1} and ω_{ρ_1} are the oscillator frequencies in the
Z and ρ directions respectively for the one centre
and ω_{Z_2} and ω_{ρ_2} are the oscillator frequencies in the Z and
ρ directions respectively for the other centre.
$U(\underline{p},\underline{s})$ the momentum dependant potential, which is a direct
generalization of the Nilsson potential, is given by:

$$U(\underline{p},\underline{s}) = -\frac{\kappa\hbar}{m\omega_0} \left\{ 2\underline{s}\cdot(\underline{\nabla}V\times\underline{p}) + \mu \left[\frac{1}{m\omega_0^2}(\underline{\nabla}V\times\underline{p})^2 - m\omega_0^2\bar{Z}^2\right] \right\} \tag{5.3}$$

Here V is the momentum independant part as given by
equation 5.2. Now if we consider only

$$H_o = \frac{-\hbar^2}{2m} \nabla^2 + V(Z,\rho)$$

it can easily be shown that the energy eigenvalues of this
Hamiltonian, for the case $\omega_{\rho_1} = \omega_{\rho_2} = \omega_\rho$, are given by :

$$E = (n_{Z_1} + \tfrac{1}{2}) \hbar\omega_{Z_1} + (N_\rho+1) \hbar\omega_\rho = (n_{Z_2} + \tfrac{1}{2}) \hbar\omega_{Z_2} + (N_\rho+1) \hbar\omega_\rho$$

where N_ρ is the quantum number of the oscillator in the
ρ direction
and n_{Z_1} and n_{Z_2} give the quantum number for the motion in
the Z direction.

By analogy with the usual Nilsson model we therefore
have for $\bar{\ell}^2$:

$$\bar{\ell}^2 = \frac{(n_{Z_1}+N_\rho)(n_{Z_1}+N_\rho+3)}{2\delta_{if}} \qquad Z \geq 0$$

$$\frac{(n_{Z_2}+N\rho)(n_{Z_2}+N_\rho+3)}{2\delta_{if}} \qquad Z \leq 0 \tag{5.4}$$

The Kronecker delta indicates that only diagonal matrix
elements of $\bar{\ell}^2$ are considered.

We can write $\bar{\ell}^2$ as :

$$\bar{\ell}^2 = \frac{N(N+3)}{2} \tag{5.5}$$

where N is identical with the principle quantum number
for $Z_{o_1} + Z_{o_2}$ = o or ∞.

The expression $(\nabla V \times \underline{p})$ in equation 5.3 can be related
to the angular momentum with respect to the two centres.
In particular for Z>o we have $\underline{\ell}_1 = \dfrac{\nabla V \times \underline{p}}{m\omega_o^2}$

and for $Z<o$ $\qquad \underset{\sim}{\ell}_2 = \dfrac{\nabla V \times \underset{\sim}{p}}{m\omega_o{}^2}$

$\qquad\qquad\qquad\qquad\qquad\qquad\qquad\qquad\qquad (5.6)$

Here $\underset{\sim}{\ell}_1$ and $\underset{\sim}{\ell}_2$ describe the angular momentum with respect to two centres at $Z = -Z_{o_1}$ and $Z = Z_{o_2}$.

This leads to the following form for the momentum-dependant potential :

$$U(\underset{\sim}{\ell},\underset{\sim}{s}) = \quad -\kappa\hbar\omega_o \left[\, 2\underset{\sim}{\ell}_1 \cdot \underset{\sim}{s} + \mu(\underset{\sim}{\ell}_1^2 - \tfrac{1}{2}N(N+3)) \,\right] \quad Z\leq o$$
$$\qquad\qquad\qquad\qquad\qquad\qquad\qquad\qquad\qquad (5.7)$$
$$-\kappa\hbar\omega_o \left[\, 2\underset{\sim}{\ell}_2 \cdot \underset{\sim}{s} + \mu(\ell_2^2 - \tfrac{1}{2}N(N+3)) \,\right] \quad Z\geq o$$

Details of the mathematical solution of equation 5.1 are given in Ref (17). There it is shown how the Hamiltonian can be diagonalized and the energy spectrum can be determined. This treatment can be carried out both for symmetrical and asymmetrical break-up. The single-particle levels thus obtained are illustrated in Fig 5.2a for symmetric break up and in Fig 5.2b for asymmetric break up.
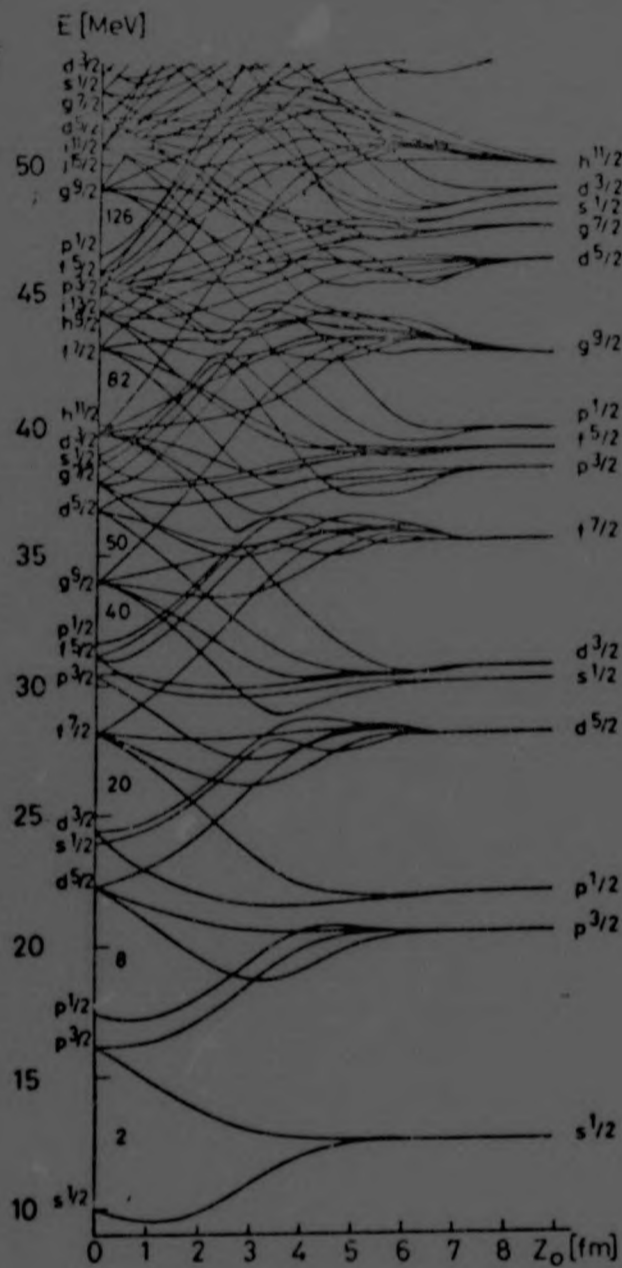
Fig. 5.2a. The single particle
levels for the symmetric break-up
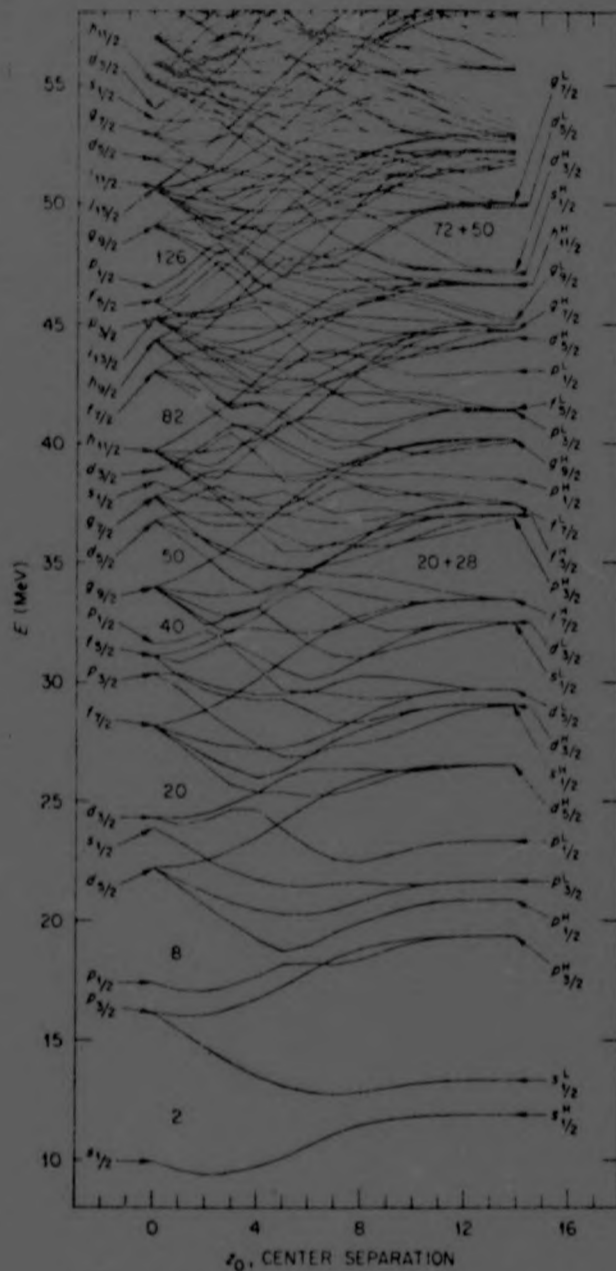in the two centre shell model.

Fig. 5.2b. The single particle
levels for the asymmetric break-
up in the two centre shell model.

The appearance of the new fragment shells, which are
doubly degenerate in the symmetric break-up case and which
lead to two different fragment shell levels in the asymmetric
break-up, is evident.

For each two-centre separation distance, $R=2Z_0$, the
single-particle energies $\varepsilon_i(R)$ of the two-centre Hamiltonian
(as given in equation 5.1) can be calculated. An instantaneous
internal energy, $U(R)$, can be got by filling the lowest states

with the number of particles in the nuclei.

$$U(R) = \sum_{i=1}^{A} \varepsilon_i(R) \tag{5.8}$$

The difference between the instantaneous value and the value when the separation is infinite yields the real nuclear part, $V(r)$, of the effective ion-ion potential at $r=R$.

$$V(R) = U(R) - U(\infty) \tag{5.9}$$

The role of the radius parameter is assumed in the two-centre oscillator by the frequency. This again allows for the possibility of distinguishing between the sudden and adiabatic processes. Setting $\omega=\omega_o$, i.e. keeping the oscillator constants unchanged during the collision, gives the sudden approximation. On the other hand, if the requirement $\omega=\omega_v(R)$, where the index v stands for volume conservation of the equipotentials, is met then the adiabatic approximation is operative.

The degree of adiabaticity or non-adiabaticity of the process can be described by parametrizing the oscillator frequency. The instantaneous oscillator frequency for separation R is given by :

$$\omega(R) = \omega_v(R) + f(E,\ell) \, (\omega_o - \omega_v(R)) \tag{5.10}$$

where $f(E,\ell)$ describes the time behaviour of the system.

$f(E,\ell)$ depends on energy E and angular momentum ℓ. For slow collisions, where the adiabatic approximation is considered to be operative, $f(E,\ell) \to o$. For fast collisions $f(E,\ell)$ tends to unity and we have the condition for the sudden approximation fulfilled.

These considerations can be applied to the case of $^{16}O-^{16}O$ scattering. The single-particle energies for the $^{16}O-^{16}O$ collision, in adiabatic and sudden approximation, are shown in Fig. 5.3.
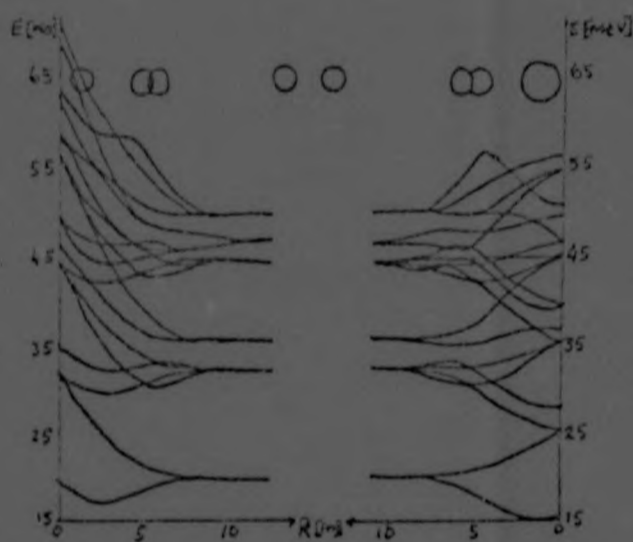

Fig. 5.3. Single particle levels for $O^{16}-O^{16}$ collisions with $\hbar\omega_0 = 13.22$ MeV and spin orbit strength $\kappa = 0.08$ as a function of relative distance R. The sudden and adiabatic cases are depicted on the left and right hand side, respectively. The levels are assigned in the order they split at large distance. The shape of the nucleus-nucleus system is shown on the top of the figure.

The corresponding nucleus-nucleus potentials for various parameter choices are shown in Fig. 5.4.
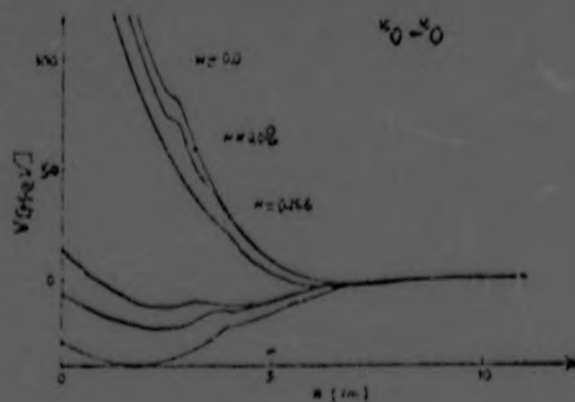

Fig. 5.4. The real nucleus-nucleus potentials for the $O^{16}-O^{16}$ system. The sudden $O^{16}-O^{16}$-potentials have at $R = 0$ the values 264.40, 239.02 and 211.73 MeV for $\kappa = 0, 0.08$ and 0.166 respectively.

The compression effect can be clearly seen in the plot of single-particle energies where most of the states have a sharp rise in energy as the separation distance tends to zero. A minimum appears in the sudden potential at a separation distance equal to about twice the nuclear radius. This can be interpreted as an attractive interaction between the nucleons at the Fermi surface.

The adiabatic potentials are expected to have a value of -35.4 MeV at R=0 in the $^{16}O-^{16}O$ case. However, the two-centre shell model is not able to correctly predict the binding energies of nuclei in either the sudden or adiabatic cases. The extended liquid drop model, however, is able to predict the binding energies. A renormalization procedure is thus employed. The extended liquid drop model is used to calculate the real part of the nucleus-nucleus potential. The shell model approach is then used to correct the extended liquid drop model potential for shell effects. A method for performing this type of renormalization was developed by Strutinsky [19] in connection with fission problems.

V.3 The Shell Correction Method

Two different single particle models are proposed. The one model is a realistic shell model having non-uniform energy spacings and level degeneracies. The other model is a smoothed-out form of the single-particle model. Here the energy spacings and level degeneracies are given a uniform distribution. The principle of the renormalization

method is that any systematic errors arising from the
general problem of calculating the total energy from a
single-particle model will be cancelled out by subtracting
the total energy of the smoothed distribution model from
that of the realistic shell model.   The remaining
contribution will then reflect the shell correction to
the smooth distribution.   This shell correction can then
be added to the liquid drop energy expression.

We see, from equation 5.8, that the realistic shell
model distribution has an energy

$$U(R) = \sum_{i=1}^{A} \varepsilon_i(R)$$

The uniform distribution, on the other hand, will
give an energy

$$\tilde{U}(R) = \int_{-\infty}^{\lambda} \varepsilon(r) \, \tilde{g}(\varepsilon) d\varepsilon \tag{5.11}$$

where $\tilde{g}(\varepsilon)$ is a uniform distribution of nucleon states and
$\tilde{\lambda}$ is the Fermi energy corresponding to $\tilde{g}$ and is determined
from the condition of number conservation

$$A = \int_{-\infty}^{\lambda} \tilde{g}(\varepsilon) d\varepsilon \tag{5.12}$$

In order to keep the uniform distribution consistent
with the overall shell distribution, the shell distribution
is averaged over an interval large enough to lose all shell
effects.   This averaging is performed by using a weighting
function.   Several different forms can be used, one of
which yields the following expression for $\tilde{g}$:

$$\tilde{g}(\varepsilon) = (\pi \gamma)^{\frac{1}{2}} \sum_{n} \exp \left[\gamma^{-2} (\varepsilon - \varepsilon_\nu)^2 \right] \tag{5.13}$$

Here the sum is over the number of levels in the energy interval $(\pi\gamma)^{\frac{1}{2}}$ centred at energy ε. If γ is taken to be of the order of the energy difference between shells then $\tilde{g}$ is no more sensitive to the exact value of γ. The energy correction is then

$$\delta U = U - \tilde{U} = \sum_{\nu=1}^{A} \varepsilon_i - \int_{-\infty}^{\lambda} \varepsilon\, \tilde{g}(\varepsilon)\, d\varepsilon \qquad (5.14)$$

Finally our corrected expression for the energy would be

$$E(R) = E_{E.L.D.M.}(R) + \delta U(R)$$

E.L.D.M. denotes extended liquid drop model. The ion-ion potential at $r = R$ is then given by

$$V(R) = E_{E.L.D.M.}(R) + \delta U(R) - E_{E.L.D.M.}(\infty) - \delta U(\infty) \qquad (5.15)$$

CHAPTER VI

The Coupled Channels Approach

VI.1   Introduction

It is possible to describe heavy-ion collisions in
terms of local potentials.   The interaction is however
better described if the potentials have both an energy and
angular momentum dependance.   Such a dependance of a potential
implies the presence of a non-local potential - a situation
to be expected in a complex many-body problem.   Now
replacing a set of coupled equations describing a system by
a single uncoupled equation leads to non-local potentials.
It is therefore not unreasonable to expect that a system of
coupled equations could lead to a good description of the
heavy-ion scattering situation.

Further, the imaginary part of the optical potential is
most important in the description of the interaction.
Since the imaginary potential is due to the coupling of the
entrance channel to the other reaction channels the explicit
inclusion of at least a few channels by means of coupled
equations should provide insight into the scattering process.
In order to do this a system of coupled Schrodinger equations
can be constructed to describe the system [20].   It then
becomes necessary to solve this system of coupled
differential equations.   If U_{ii} is the diagonal potential
for the ith channel and U_{ij} is the coupling potential
between the ith and jth channels we have :

$$(T + c_i - E + U_{ii}) \phi_i = \sum_{\substack{j=1 \\ j=i}}^{N} U_{ij} \phi_j \quad i=1,2,\dots,N \quad (6.1)$$

The advantage of postulating such a system is that the wave functions are solved simultaneously for the elastic and the strongly coupled inelastic channels. Such calculations however are complicated and in general are simplified by restricting the number of coupled channels available. Rawitscher [21] has performed calculations for $^{16}O-^{16}O$ where the only allowed excitation is the 1^- excitation which was supposed to represent the 3^- 6.14 MeV state in ^{16}O. Further interest in the use of coupled equations was stimulated by the proposition [22] that much of the intermediate structure in the excitation functions for heavy-ion collisions can be explained in terms of transitions between quasibound and virtual states of a quasimolecule.

VI.2 The Double-Resonance Effect

When two nuclei collide against each other there will be an attraction at the surface of their density distributions due to the long range part of the nuclear forces. There will at the same time be forces tending to separate the nuclei arising from their rotation and the repulsive centrifugal barrier. When all these forces are in equilibrium the possibility of having a nuclear molecule exists [23].

Fig. 1 shows the typical form of the real potential in heavy-ion scattering.
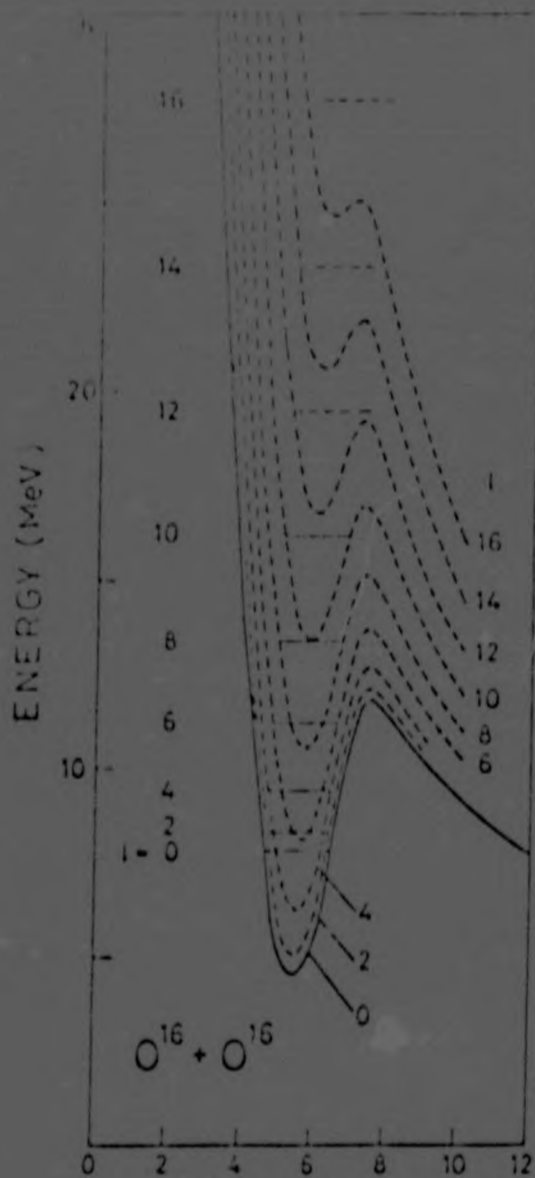
Fig. 6.1.   The real potential for O^{16}-O^{16}-scattering in the sudden approximation.   The centrifugal potential is included.   The virtual states ($\ell > 12$) are shown as dashed horizontal lines, while the quasibound states ($\ell < 10$) are full horizontal lines.   The position of these states has been chosen such that the nuclear phase shift has the value $\delta_\ell = \pi/2$ at these energies.   The phase shifts are obtained from a phase shift analysis.

The nucleus-nucleus system may perform stable rotations and vibrations in these potentials.   A requirement for such rotations to occur with angular momentum ℓ at a separation distance b is:

$$\frac{d}{dr}\left(V(r) + \frac{\ell(\ell+1)\,\hbar^2}{2\mu r^2}\right)\Bigg|_{r=b} = 0 \qquad (6.2)$$

The potential thus contains states up to a certain

maximum angular momentum state. These states are called
quasibound and are denoted by full lines in Fig. 6.1. Those
states which lie above this maximum angular momentum as
determined by equation 6.2 are called virtual states and are
denoted by dashed lines.

The importance of a coupled channels calculation in
this approach lies in the concept of a double-resonance effect.
It is not possible to directly excite the quasibound states
in an elastic scattering collision because of the impenetrability
of the potential barrier. However, virtual excitations of
these quasibound states is possible if we allow for a double
resonance. If the ions are incident with energy E_i and
lose kinetic energy E^* by inelastic excitations after they
have crossed the potential barrier they will be able to form
a quasi-molecule if their relative energy E_i-E^* coincides
with the energy of a quasibound state. For such a process
to occur it is necessary however for the inelastic and
elastic channels to be sufficiently strongly coupled among
each other, but only weakly coupled to the compound states.

VI.3   The Hamiltonian of the Model

The Hamiltonian describing the scattering of two nuclei
can be written as :

$$H = T_r(r) + H_1(1) + H_2(2) + W(r,1,2) \qquad (6.3)$$

where T_r describes the kinetic energy of the relative motion.
H_1 and H_2 are the intrinsic Hamiltonians of the two nuclei and
$W(r,1,2)$ is the interaction energy for the two nuclei.

The interaction can be expanded in spherical harmonics.

$$W(r,1,2) = U(r) + \sum_{\ell,m} (1)^m Q_{\ell m}(r,1,2) Y_{\ell -m}(\Omega) \qquad (6.4)$$

$U(r)$ is the average optical potential between the nuclei. $Q_{\ell m}$ couples the relative and intrinsic motion.

The eigenstates of the individual nuclei are the solutions of the intrinsic Hamiltonians :

$$H_i(i) \chi_{\alpha i}(i) = \varepsilon_{\alpha i} \chi_{\alpha i}(i) \qquad i=1,2 \qquad (6.5)$$

α_i represents the set of quantum numbers describing the particular states.

The solution ψ of the Hamiltonian 4 can be expressed [20] as :

$$\psi = \sum_{\ell,J,\lambda,I} R_{\ell J \lambda I}(r) \left[i^\ell Y_\ell(\Omega) \times \phi_{J\lambda}(1,2) \right]^{(I)} \qquad (6.6)$$

with the channel wave function :

$$\phi_{J\lambda}(1,2) = \left[2(1+\delta_{\alpha_1 \alpha_2}) \right]^{-\frac{1}{2}} \left[\chi_{\alpha_1}(1) \times \chi_{\alpha_2}(2) + (-)^\ell \chi_{\alpha_1}(2) \times \chi_{\alpha_2}(1) \right]^{(J)}$$

$$\lambda = (\alpha_1, \alpha_2) \qquad (6.7)$$

It is now necessary to symmetrize the channel wave function with respect to the exchange of the two nuclei. The wave function is symmetrized in the entrance channel and, since the Hamiltonian conserves symmetry, only symmetrized intrinsic wave functions can couple with the entrance channel.

Applying the Schrodinger equation, the set of functions 6.6 and 6.7 give rise to a set of coupled equations. Integrating over the intrinsic coordinates and the angle Ω of the relative distance gives :

$$\langle i^{\ell}[Y_{\ell} \times \phi_{J\lambda}]^{(I)}|H|\psi\rangle = E \langle i^{\ell}[Y_{\ell}\times\phi_{J\lambda}]^{(I)}|\psi\rangle \qquad (6.8)$$

These matrix elements reduce to :

$$\left[\frac{-\hbar^2}{2\mu} \frac{1}{r^2} \frac{d}{dr} r^2 \frac{d}{dr} + U(r) + \frac{\ell(\ell+1)\hbar^2}{2\mu r^2} + \varepsilon_{\alpha_1} + \varepsilon_{\alpha_2} - E\right] \times R_{\ell J\lambda I}(r)$$

$$= -\sum_{\ell',J',\lambda',L} i^{\ell-\ell'}(-)^{\ell'+I+J} \left\{ \begin{matrix} I & J & \ell \\ L & \ell' & J' \end{matrix} \right\} \langle \ell|Y_{\ell}|\ell'\rangle\langle J\lambda|Q_L|J'\lambda'\rangle R_{\ell'J'\lambda'I}(r)$$

$$\qquad (6.9)$$

This set of equations can be restricted to account only for those channels which couple strongly to the entrance channel. By making simplifying assumptions on the nature of the excited states it is possible to derive the following expression for the transition where an ^{16}O nucleus in the state $\mu_1 = (I_1, M_1, n_1)$ is incident on an ^{16}O target in the state μ_2 [24].

$$\left(\frac{d\sigma}{d\Omega}\right)_{\mu_1,\mu_2 \to \mu_1',\mu_2'} = \left| f_c(\theta)\delta_{\mu_1\mu_1'} \delta_{\mu_2\mu_2'} + f_c(\pi-\theta) \delta_{\mu_1\mu_2'} \delta_{\mu_2\mu_1'} \right.$$

$$+ \sum_{\ell,\ell';m;J,M_J,J',M_{J'}} \frac{i[\pi(2\ell+1)]^{\frac{1}{2}}}{k} (I_1M_1I_2M_2|JM_J)$$

$$\times (I_1'M_1'I_2'M_2'|J'M_{J'}) (\ell 0 JM_J|IM) (\ell'm'J'M_{J'}|IM)$$

$$\times \left[(1+\delta_{\alpha_1\alpha_2})(1+\delta_{\alpha_1'\alpha_2'})\right]^{\frac{1}{2}}(e^{2i\eta_\ell} \delta_{\ell\ell'}\delta_{JJ'}\delta_{\lambda\lambda'} - \delta_{\ell'J'\lambda',\ell J\lambda})$$

$$\left. \times Y_{\ell'm'} \right|^2 \qquad (6.10)$$

One of the nuclei is measured in the state μ_1' in the direction θ, the other is measured in the opposite direction in the state μ_2'.

VI.4 Comparison with Experiment

The model has been applied as an illustrative example to the case of ^{16}O-^{16}O scattering between 19 and 22.5 MeV [24].

The real potential was taken to be as calculated in the
extended liquid drop model in sudden approximation.

Only the excitation of the 3^- and 2^+ states in one
individual nucleus was considered. Therefore for every
total angular momentum I the eight channels given below
were considered :

elastic $\qquad \ell = I$

inelastic $3^- \qquad \ell = I-3, I-1, I+1, I+3$

inelastic $2^+ \qquad \ell = I-2, I, I+2$

The following forms were taken for simplicity for the
reduced matrix elements.

The $\langle J\lambda|Q_J|0\rangle$ were taken to be constant

$$\langle 2^+|Q_2|0\rangle = C_2 \theta(1-\tfrac{r}{a})$$

and $\langle 3^-|Q_3|0\rangle = C_3 \theta(1-\tfrac{r}{a})$

where $a = 7$ fms and the constants C_2 and C_3 are taken
from experiment.

As the relative energy of the nuclei becomes quite
small after a collision the quasibound molecules exist at an
energy where only few compound states exist. One therefore
expects only small volume absorption. A surface peaked
imaginary potential is consequently chosen for the inelastic
channels.

$$W_{inel} = W_o \frac{(4(r-r_a)(r_b-r))^2}{(r_b-r_a)^2} \qquad r_a \leq r \leq r_b$$

$$= 0 \qquad\qquad r < r_a \text{ or } r > r_b$$

Matching to the inelastic cross-section required

$r_a = 7.3$ fm, $r_b = 9.0$ fm and $W_0 = 4$MeV.

Fig. 6.2 shows the potentials used in the calculation
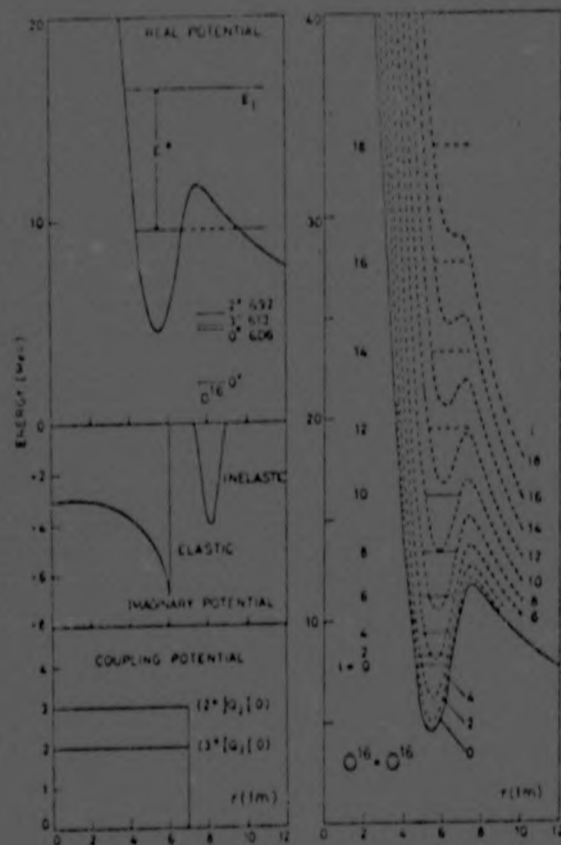of the intermediate structure in the $^{16}O - ^{16}O$ interaction.

Fig. 6.2. Summary of the potentials used in the calculation for
intermediate structure in the $O^{16} - O^{16}$-scattering between 19 and 22 MeV.

Fig. 6.3 shows the calculated excitation function for the
elastic and inelastic $^{16}O - ^{16}O$ scattering in the energy interval
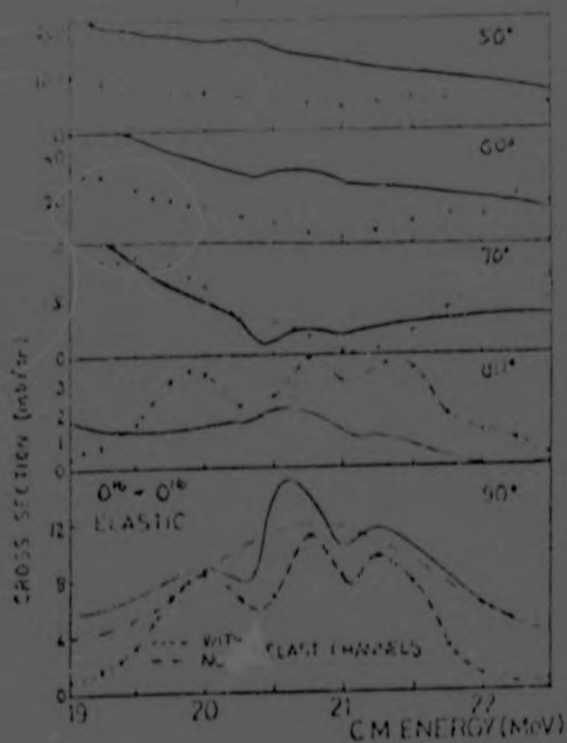19 to 22.5 MeV in comparison with experiment.

Fig. 6.3. Elastic differential scattering cross sections at various angles. The theoretical curves are obtained with the potentials of figure 24. Only the 3⁻(6.13 MeV) and the 2⁺(6.92 MeV) states of O¹⁶ are considered in the excitation mechanism. The first and second minimum in the elastic 90° excitation function are caused by the excitation of the 2⁺ and 3⁻-state, respectively.

Because of the double resonance mechanism the presence of coupling gives rise to intermediate structure of width about 100 keV in the excitation function. Such structure is not predicted in optical model calculations. For a coupling model to provide a full description of a heavy-ion scattering process it is however necessary to determine all channels which will contribute to the cross-section and include them in the coupled equations.

CHAPTER VII

Microscopic Calculations of the Imaginary Potential

VII.1 Introduction

We have seen that the addition of an imaginary part
into the optical potential provides models able to give
reasonable agreement with experimental results.   In
particular Chatwin et al provided a semi-phenomenological
angular momentum dependant imaginary potential which
provided a much improved optical potential.   However these
potentials are seen to give agreement with experiment only
over a limited range.   It was also found that the introduction
of a parametrized energy-dependance for the imaginary part
of the potential gives closer agreement with experiment.
However such potentials are not unique.   Microscopic
approaches have therefore been made to derive a parameter
free imaginary potential.

VII.2 Consideration of Transitions from Elastic to Inelastic
Channels.

Prüss [25] has shown from formal aspects of reaction
theory that the Hamiltonian of an A-nucleon system in the
centre-of-mass frame,

$$H = T + \sum_{i<k} V_{ik} - T_{C.M.} \tag{7.1}$$

where $T_{C.M.}$ is the kinetic energy of the centre of mass,
can be reduced to the optical model for elastic scattering

between two nuclei

$$H = T+U - i \sum_{\ell,m} W_\ell |Y_{\ell m}\rangle\langle Y_{\ell m}| \tag{7.2}$$

where $U(r) = \dfrac{1}{\sqrt{4\pi}} \langle \phi_0 |Q| \phi_0 \rangle$ \hfill (7.3)

and $W_\ell(r) = \pi \sum \dfrac{|\langle \ell 0|V|\ell k\rangle|^2}{2\ell+1} \rho_{J\lambda} \left(E - \dfrac{\ell'(\ell'+1)\hbar^2}{2\mu r^2} \dfrac{\langle \ell k|V|\ell k\rangle}{\sqrt{2\ell+1}}\right)$

$$\tag{7.4}$$

Here Q is the projection operator onto the non-elastic channels and ϕ_0 arises as the solution of the non-elastic part of the total wave function.

$\rho_{J\lambda}$ is the density of states $\phi_{J\lambda}$.

A consideration of the transition probability from elastic into inelastic channels [26] provides a more tractable form for the imaginary potential 7.4.

The transition probability for decay from the molecular state into the compound states of density $\rho_{J\lambda}(E^*)$ is given in first-order perturbation theory by the golden rule:

$$\dfrac{(\Gamma_\ell)}{\hbar}_{e\ell} = \dfrac{2\pi}{\hbar} \rho_{J\lambda}(E^*) \, |\langle \text{compound}\,|V|\,\text{elastic}\rangle|^2_{\text{average}}$$

$$\tag{7.5}$$

and the imaginary potential W is given by:

$$W_\ell = -i\Gamma_\ell \over 2 \tag{7.6}$$

The imaginary potential can be seen to be proportional to the density $\rho_{J\lambda}(E^*)$ of the states $\phi_{J\lambda}$. It is thus clear that the imaginary potential shows a strong angular momentum and energy dependance.

To apply formula 7.5 it is necessary that the width
of the inelastic states should be large compared to the
average level spacing so that statistical approximations
for the level densities are valid and the transition matrix
elements can be averaged. Since only a few inelastic
channels are open at higher angular momentum these
conditions will not be fulfilled and it is then necessary
to treat these channels explicitly in a coupled channels
calculation.

Calculations of the imaginary potential have been
performed [26] on the basis of equations 7.5 and 7.6.

A typical time period for heavy-ion collisions is
of the order 5×10^{-22} secs. In this period a precompound
nucleus can be considered to be formed which will be the
doorway state for all inelastic processes. After about
10^{-18} seconds statistical equilibrium is reached and the
compound nucleus formed. Our expression 7.6 for the
imaginary potential describes the formation of the
precompound nucleus. Equations 7.5 and 7.6 are valid
only in a never-come-back approximation. To further
simplify the problem the compound and precompound nuclei
are considered to have the same level density given by :

$$\rho_\ell(E^*) = c \, \exp\left[2\sqrt{aE^*}\right] \frac{(2\ell+1)}{2\sigma^2} \, \exp\left[\frac{-(\ell+1)^2}{2\sigma^2}\right] \quad (7.7)$$

The excitation energy of the compound states E^* is
given by summing the bombarding energy and the difference in
the binding energy of the compound system and of the two
incident nuclei.

For a given excitation energy an upper limit of the
angular momentum, the yrast level, exists for the compound
states.   This highest angular momentum is assumed to be
that for which all the energy E^* is transformed into
rotational energy.

$$E^* = \ell_{max} (\ell_{max} +1) \frac{\hbar^2}{2\theta}$$

(7.8)

θ is the moment of inertia and is assumed to be constant.
The cut-off parameter σ in equation 7.7 is chosen so that
the exponential function in equation 7.7 decreases to the
value $\frac{1}{e}$ for $\ell = \ell_{max}$.   This leads to a linear dependance of
σ^2 on E^*

$$\sigma^2 = \frac{\theta E^*}{\hbar^2}$$

(7.9)

An accurate determination of the radial dependance
of the matrix element which arises in equation 7.5 can only
be derived from an explicit single-particle model.   However
a simple and plausible radial dependance can be provided by
setting the square of the average matrix element proportional
to the number of nucleons in the region of overlap between
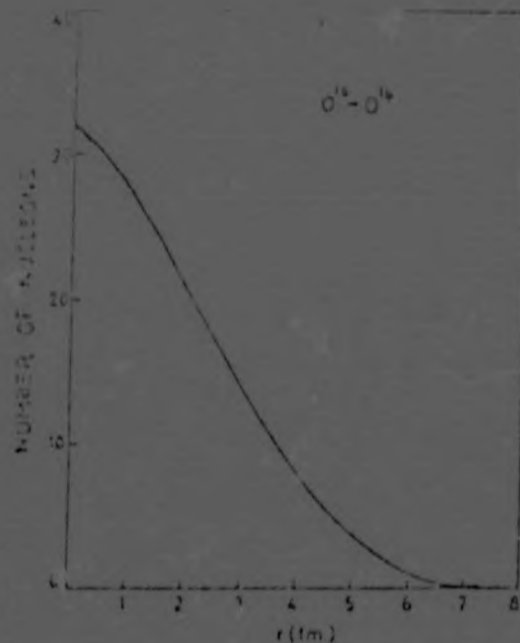the two colliding nuclei.

Fig. 7.1. The number of nucleons contained in the region where the densities of the two ^{16}O-nuclei overlap as function of the relative distance between the two centres of the ^{16}O-nuclei.

The imaginary potential, given by equation 16, becomes by use of equations 7.5 and 7.7 :

$$W_\ell = -i a \exp \left[2 \sqrt{aE^*} \right] \frac{2\ell+1}{2\beta E} \exp \left[\frac{-(\ell+1)}{2\beta E} \right]^2 \int \rho d\tau \bigg|_{\text{overlap}} \qquad (7.10)$$

where $\beta = \dfrac{\theta}{\hbar^2}$

and the parameter a·is given by :

$$a = 0.0035(A-12) \text{ MeV}^{-1} \text{ for } 15<A<70$$

The parameters a and β are adjusted for the particular nuclei in the experiment. For example the values found by Helling et al [26] for ^{16}O- ^{16}O scattering were

$$a = 1.1 \times 10^{-3} \text{ MeV and } \beta = 1.9 \text{ MeV}^{-1}$$

The use of such a potential is able to reproduce the excitation function quite well up to an energy of about 35 MeV. (Fig. 7.2) :
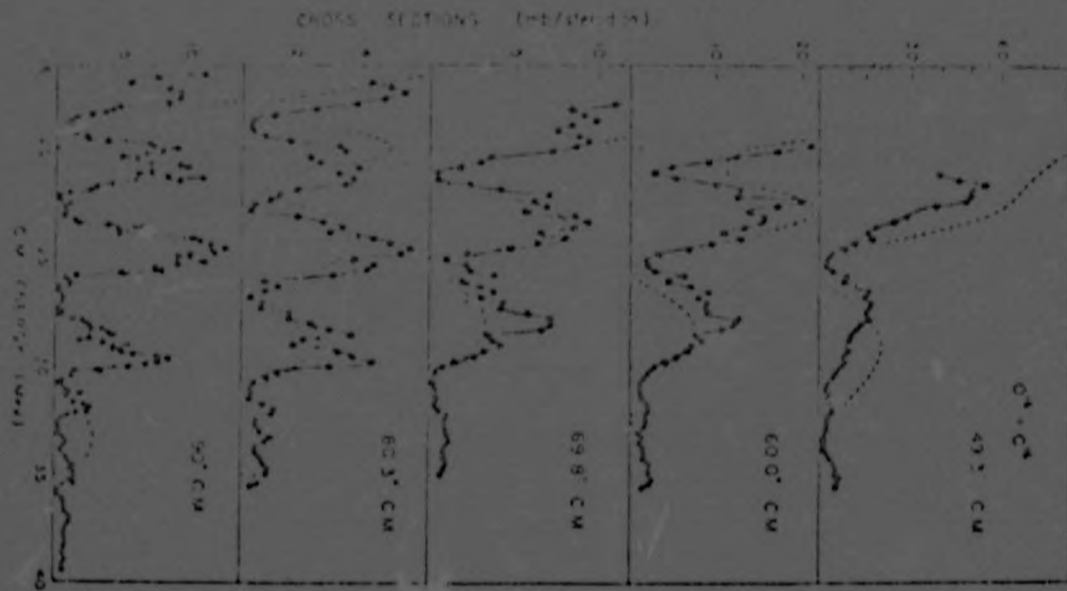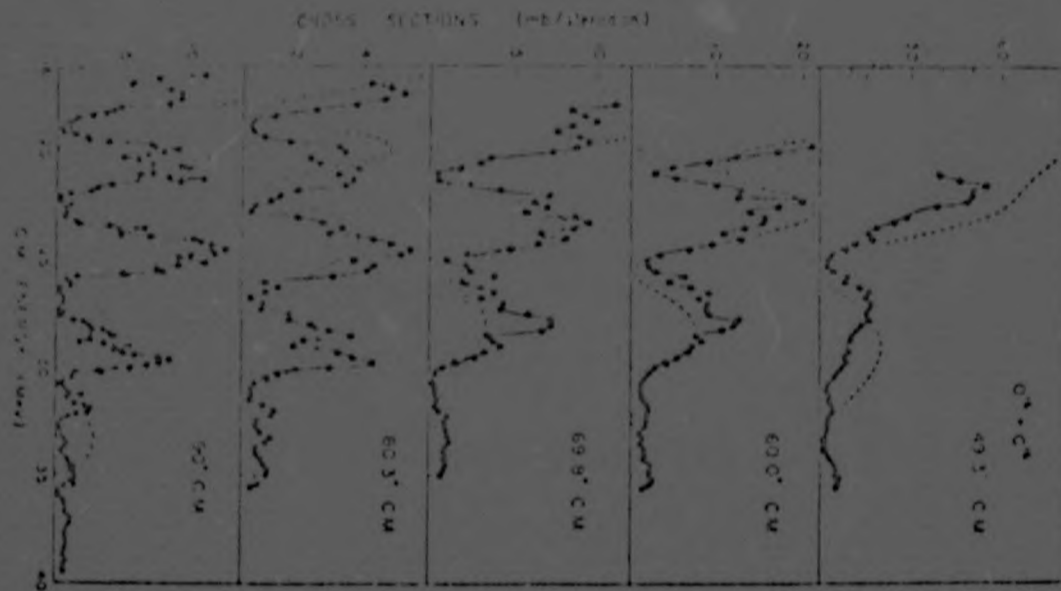
Fig. 7.2. The excitation functions for the elastic scattering of
^{16}O on ^{16}O. The experimental points are measured at 49.3°, 60°,
69.8°, 80.3° and 90° by the Yale-Group. The theoretical curve is
calculated with the Yale real potential and with the absorptive
potential according to eq.7.10. The parameters of the absorptive
potential are found as $\alpha=1.1 \times 10^{-3}$ MeV and $\beta=1.9$ MeV^{-1}. The cross
section shows the correct peak-to-valley ratio and decreases
sufficiently at higher bombarding energies.

VII.3 Dynamic Absorption Model

The starting point for this model [27] is Goldberger's
"frivolous scattering model" which describes the absorption
of free nucleons in nuclei.

It is possible to describe the nucleus as a refractive
medium with complex refractive index for an incident nucleon.
The refractive index η, is determined by the energy, E, of
the incident nucleon and the optical potential V+iW

$$\eta = \sqrt{\frac{E-(V+iW)}{E}} \qquad (7.11)$$

Fig. 7.2. The excitation functions for the elastic scattering of ^{16}O on ^{16}O. The experimental points are measured at 49.3°, 60°, 69.8°, 80.3° and 90° by the Yale-Group. The theoretical curve is calculated with the Yale real potential and with the absorptive potential according to eq.7.10. The parameters of the absorptive potential are found as $\alpha = 1.1 \times 10^{-3}$ MeV and $\beta = 1.9$ MeV^{-1}. The cross section shows the correct peak-to-valley ratio and decreases sufficiently at higher bombarding energies.

VII.3 Dynamic Absorption Model

The starting point for this model [27] is Goldberger's "frivolous scattering model" which describes the absorption of free nucleons in nuclei.

It is possible to describe the nucleus as a refractive medium with complex refractive index for an incident nucleon. The refractive index η, is determined by the energy, E, of the incident nucleon and the optical potential V+iW

$$\eta = \sqrt{\frac{E-(V+iW)}{E}} \tag{7.11}$$

If the incident nucleon has momentum

$$k = \sqrt{\frac{2\mu E}{\hbar^2}} \qquad (7.12)$$

then inside the nucleus it will have

$$k + k_1 + i\frac{\kappa}{2} = \sqrt{\frac{2\mu(E_{C.M.} - V - iW)}{\hbar^2}} \qquad (7.13)$$

where κ is the absorption coefficient.

From this one gets the relationship

$$W = \frac{\hbar^2}{2\mu}\kappa\sqrt{\frac{\kappa^2}{4} + \frac{2\mu}{\hbar^2}(E_{C.M.} - V)} \qquad (7.14)$$

Other authors [28] use the semi-classical form for W,
given by :

$$W(\underline{r}_1,\underline{R}) = \frac{1}{2}\hbar v(\underline{r}_1,\underline{R})\kappa$$

where v is the velocity of an incident nucleon.

In order to calculate κ or its inverse, the mean free
path λ, one considers the colliding nuclei in phase space
where they occupy restricted six-dimensional regions separated
by the distance vector $\underline{R}$ and the relative momentum per
nucleon $\underline{K}$. Fermi-type mass distributions are assumed.
The intrinsic momentum is determined by associating a Fermi
sphere, whose radius k_F is determined by the compound mass
density ρ, with every point. The relationship between the
Fermi momentum and the density will be derived in the section
on the energy dependant real potential. It is found that

$$k_F^2(\underline{r},\underline{R}) = \left(\frac{3}{2}\pi^2\rho\right)^{2/3} + \frac{5}{12}\xi\left(\frac{\nabla\rho}{\rho}\right)^2 \qquad (7.15)$$

where the second term is an inhomogeneity correction and
$\xi = \frac{1}{9}$.

The compound density can be calculated in either
the sudden or the adiabatic approximation. It turns out
that the dynamical absorption model depends only weakly
on the degree of adiabaticity or suddenness present for
the reaction process since the dominant factor is the
collective momentum K.

As the colliding nuclei begin to overlap, 2p-2h states
will be created by the scattering of nucleons into states
outside the Fermi spheres. Both inelastic excitations
and transfer processes can arise from these states which
can be regarded as the doorway states for all non-elastic
channels. In particular thermalization leads to compound
states. The absorption coefficient κ i therefore
determined by the formation cross section $\bar{\sigma}$ of these
doorway states. One can obtain κ as a function of K and R
by folding this formation cross-section, $\bar{\sigma}$ (r,R,K), with
the densities of the scattering nuclei at all points r.

$$\kappa (R,K) = \int d^3r \; \rho_1(r)\rho_2(R-r) \; \bar{\sigma} (r,R,K) \qquad (7.16)$$

The formation cross-section can be calculated by
averaging the cross-section for elementary collision of
bound nucleons $\sigma_b(k)$ over the intrinsic momentum
distributions at the position r of the scattering event.
One must take into account that the scattering centres are
in relative motion. The formation cross-section is then :

$$\bar{\sigma}(r,R,K) = |V_F(r)|^{-2} \int d^3k_1 \int d^3k_2 \; \frac{2k}{K} \; \sigma_b(k) \qquad (7.17)$$
$$F_1(r) \quad F_2(r)$$

where $V_F = \frac{4}{3} \pi k_F^3$ is the volume of the Fermi spheres F_1
and F_2 which are separated by the momentum per nucleon $\underline{K}$.
k_F is calculated with the compound density 7.15.

$\underline{k} = \frac{1}{2}(\underline{k}_1 + \underline{K} - \underline{k}_2)$ is the relative momentum of the
scattering nucleons.

The factor $\frac{2k}{K}$ is introduced to allow for the relative
motion of the scattering centres.

The microscopic cross-sections $\sigma_b(k)$ describe the
interaction of bound nucleons within the nuclei. They
can be derived from the data for free nucleon-nucleon
scattering $\sigma_F(k)$ by integrating the free nucleon-nucleon
scattering cross-sections over all directions of the final
relative momentum, which lead to states which are allowed
by the Pauli exclusion principle

$$\sigma_b(k) = \int_{\Omega_b} \sigma_F(\underline{k},\underline{k}') \, d\Omega_{\underline{k}'} \tag{7.18}$$

Geometrical considerations determine the region of
space allowed by the Pauli principle and hence the solid
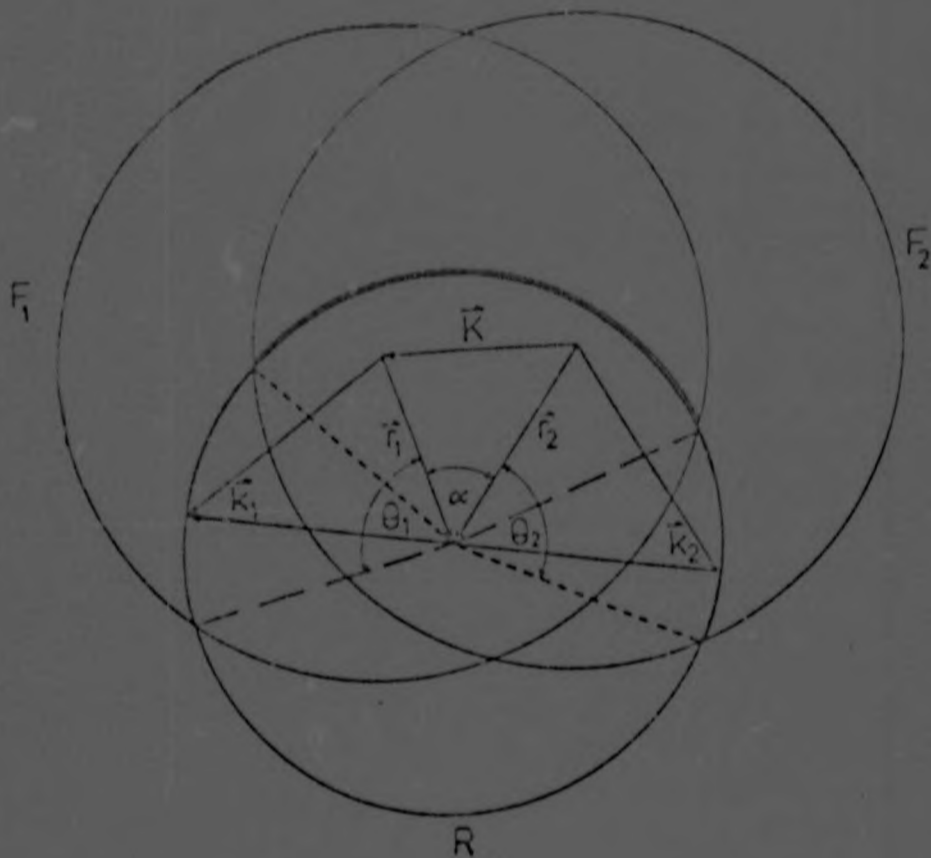angle Ω_b. Consider the interaction of Fermi sphere F_1
with Fermi sphere F_2.

Fig.7.3 The Fermi spheres F_1 and F_2 separated by momentum K and intersected by the auxiliary sphere R. θ_1 and θ_2 are the angles of the spherical cones cut out of F_1 and F_2.

Energy and momentum conservation require that the endpoint of $\underline{k}'$ must fall on a sphere $\underline{R}$ with radius k which cuts two spherical cones out of F_1 and F_2 (Fig. 7.4)

The states in the intersection of these cones are already occupied in both nuclei. Scattering is therefore forbidden into this region and, since the colliding nucleons cannot be distinguished, into the region which one obtains by reflection at the origin of $\underline{R}$.

The set of energy-dependent imaginary potentials for $^{16}O-^{16}O$ scattering is shown in Fig. 7.5

The origin of the energy dependence of the absorption can be understood from a consideration of the situation in momentum space (Fig. 7.3). An increase in the relative momentum k leads to a decrease in the Pauli-forbidden overlap region between F_1 and F_2. More phase space is thus made available after the collisions and the absorption becomes stronger.

The shape of the radial dependance of the imaginary potential follows the form of the overlap density. W turns out to be both surface transparent and strongly absorbing in the inner region in this model.

The $^{18}O-^{18}O$ system has a larger aggregate radius than the $^{16}O-^{16}O$ system and is more diffuse. The overlap density is dependant on these parameters and the diffraction model correspondingly predicts a stronger absorption and damping of the gross structure for the $^{18}O-^{18}O$ system, as is observed.
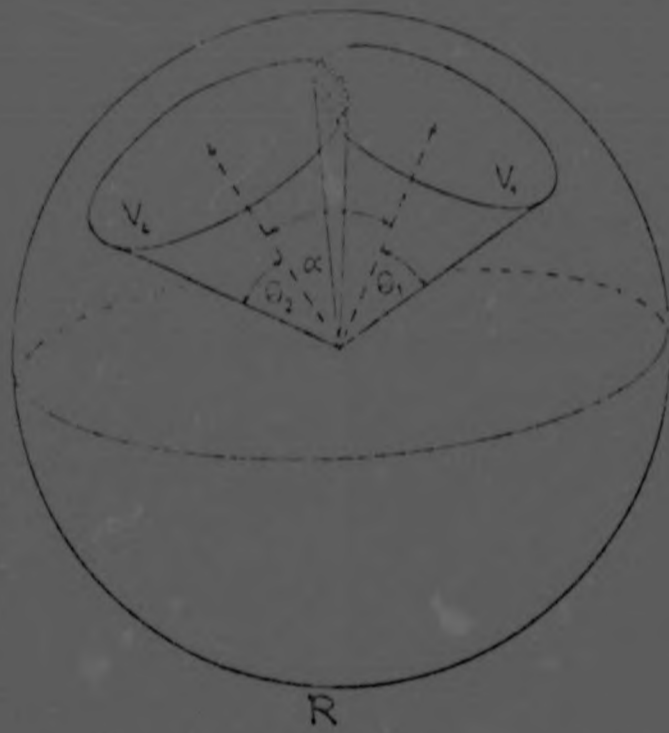
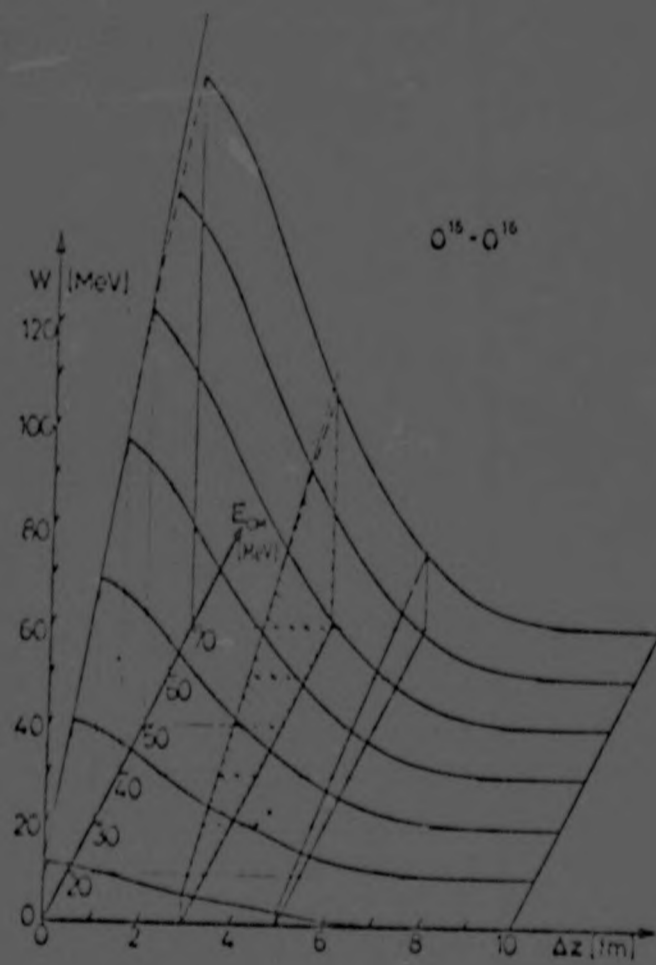Fig. 7.4 The two spherical cones.   The shaded area is the Pauli-
forbidden region.

Fig. 7.5 Imaginary potential for $^{16}O-^{16}O$ scattering

CHAPTER VIII

Folding models for ion-ion collisions

VIII.1 Introduction

The success of the investigations [29] into the single
nucleon-nucleus optical potential applying a folding
potential led to a similar philosophy being adopted for
the treatment of the optical potential in heavy-ion
scattering. In the single nucleon optical potential
investigations the nucleon-nucleus optical potential is
obtained by summing all the individual internucleon
potentials and is given by

$$V(\underline{r}) = \int v(\underline{r}-\underline{r}') \, f(\underline{r}') \, d^3r' \qquad (8.1)$$

where $f(\underline{r}')$ is the density of the nucleons in the
nucleus and $v(\underline{r}-\underline{r}')$ is the nucleon-nucleon interaction
potential.

It is possible to extend this approach to the case of
heavy-ion interactions [30].

VIII.2 Nucleus-Nucleus Potential from a Phenomenological
Nucleon-Nucleus Potential

The Feshbach formulation of the optical potential
allows for both direct and exchange terms in the interaction
between two nuclei. The direct term describes processes
involving the elastic channel only and yields a real local
potential. The exchange terms, however, involve inelastic

channels and yields a non-local potential containing the
imaginary part of the optical potential.   In the single
nucleon optical potential it is shown that in general the
exchange terms are small compared with the direct terms and
that the direct term is given to a good approximation by
folding the nucleon-nucleon potential with the nuclear
matter distribution:

The nucleus-nucleus potential is written as:

$$V_{12}(R) = \int \rho_1(r_1) \, V_2 \, (r_1 - R) d^3 r_1 + \text{exchange} \qquad (8.2)$$

where $\rho_1(r_1)$ is the density of nucleus 1

and $V_2 \, (r_1 - R)$ is the real part of the single nucleon
optical potential for nucleus 2.

For large separations of the nuclei the overlap of
the nuclei will be small.   Since the exchange term arises
from the antisymmetrisation requirement for the two-nucleus
wave function, it too will be small.   The philosophy
adopted in Ref. (30) is to calculate a maximum angular
momentum L_c for which the top of the nucleus-nucleus
potential barrier coincides with the incident energy.
Predictions about the scattering cross-section are then
made in terms of diffraction mode's employing this value
of L_c.   The potential need then only be calculated up to
the Coulomb barrier and in this event the neglect of the
exchange term is considered to be a reasonable approximation.

The long range part of the nucleus-nucleus interaction
is then given by :

$$V_{12}(R) = \int \rho_1(r_1) \, V_2(r_1 - R) \, d^3 r_1 \qquad (8.3)$$

When ρ_1 and V_2 both have spherical symmetry the integral reduces to a two-dimensional integral over r_1 and r_2.

$$V_{12}(R) = \frac{2\pi}{R} \iint \rho_1(r_1) \, V_2(\quad) \, r_1 r_2 \, dr_1 dr_2 \qquad (8.4)$$

The limits of integration are fixed by the triangular conditions :

$$r_1 + r_2 > R \qquad |r_1 - r_2| < R$$

The density distribution ρ_1 and the interaction V_2 are assumed to have Saxon-Woods forms having the same thickness parameters but different radius parameters in order to derive analytical solutions to equation 8.4.

The forms assumed are :

$$\rho_1(r) = \frac{\rho_o}{1 + \exp\left(\frac{r - R_1}{T}\right)}$$

$$V_2(r) = \frac{V_o}{1 + \exp\left(\frac{r - R_2}{T}\right)} \qquad (8.5)$$

By a suitable change of coordinates the integration reduces to :

$$V_{12}(R) = \frac{\pi \rho_o V_o}{4R} \int_R^\infty I(s) \, ds \qquad (8.6)$$

with $I(s) = \int_{-\infty}^\infty dt \, (s^2 - t^2) \left[1 + \exp\left(\frac{s + t - 2R_1}{2T}\right)\right]^{-1} \left[1 + \exp\left(\frac{s - t + 2R_2}{2T}\right)\right]^{-1}$

This integration can be performed analytically to give

$$I(s) = \frac{(s - [R_1 + R_2]) \, (2s^2 - \frac{8\pi^2 T^2}{3}) - \frac{1}{3} \left[(s - 2R_1)^3 + (s - 2R_2)^3\right]}{\exp\left(\frac{s - [R_1 + R_2]}{T}\right) - 1}$$

Using this expression for $I(s)$ the integral in
equation 8.1 was carried out numerically and the desired
parameter L_0 was then obtained.

In this procedure each nucleon of the projectile is
treated as being free and the perturbation felt by each
nucleon in the projectile as a result of the field of all
other nucleons is neglected.   This disregards the
saturation properties of the two-body interaction.   An
alternative scheme has been proposed [31] which takes into
account the two-body saturation properties.

VIII.3 Use of a Density-Dependant Two-Body Interaction

The introduction of a density-dependance in the two-
body interaction approximately takes care of the saturation
properties of this interaction.   The method employed in
Ref. (31) to calculate the nucleus-nucleus potential therefore
folds in a density-dependant two-body effective interaction
with the target density to obtain the nucleon-nucleus
potential.   The nucleon-nucleus potential obtained in this
way is then folded in with the projectile density to give
the ion-ion potential.

In a nucleus-nucleus interaction each nucleon in the
projectile is embedded in a nuclear medium.   The local
density in the two-body interaction therefore should be
computed taking into account the contribution of the density
from both the target and the projectile.

A suitable linear density-dependant interaction was
used by Lande et al [32] to obtain the following form for
the single nucleon optical potential at a point $\underline{t}$ relative
to the centre of the target :

$$U_i(t) = \sum_{i=p,n} \rho_1^i(\xi_1) \; V_{k-k}^i(|\underset{\sim}{s}|)\alpha^i \; \{1-\beta^i[\rho_{m1}(\underset{\sim}{x})+\rho_{m2}(\xi_2+\tfrac{1}{2}\underset{\sim}{s})]\}d^3\xi_1$$

$$(8.8)$$

$$(i = proton, neutron)$$

Here the exchange effects between target and projectile nucleons are neglected. V_{k-k} is the Kallio-Koltveit form for the nucleon-nucleon interaction. α^i and β^i are parameters given in Ref (32). The target is centred at ξ_1 with nucleon density distribution ρ_1^i. [In] equation 8.8 $\underset{\sim}{x} = \tfrac{1}{2}(\underset{\sim}{r}+\xi_1)$ and $|\underset{\sim}{s}| = |\underset{\sim}{r}-\xi_1|$. ρ_{m1} and ρ_{m2} denote the target-matter and projectile-matter densities respectively.

An expansion is made of $\rho_{m2}(\xi_2+\tfrac{1}{2}\underset{\sim}{s})$ about ξ_2 to give

$$\rho_{m2}(\xi_2+\tfrac{1}{2}\underset{\sim}{s}) = \rho_{m2}(\xi_2)+ \frac{1}{24} \; s^2\nabla^2\rho_{m2}(\xi_2) \qquad (8.9)$$

This is substituted into 8.8 to give :

$$U(\underset{\sim}{R}) = \int\rho_{m2}(\xi_2) \; U_{11}|\underset{\sim}{R}-\xi_2| \; d^3\xi_2 - \int\rho_{m2}^2(\xi_2)U_{12}|\underset{\sim}{R}-\xi_2|d^3\xi_2$$

$$- \int\rho_{m2}(\xi_2) \; \nabla^2 \; \rho_{m2}(\xi_2) \; U_{13}|\underset{\sim}{R}-\xi_2| \; d^3\xi_2 \qquad (8.10)$$

where U_{11}, U_{12} and U_{13} have the following forms :

$$U_{11}(t) = \sum_{i=p,n} \int\rho_1^i(\xi_1) \; V_{k-k} \; (|\underset{\sim}{s}|)\alpha^i[1-\beta^i\rho_{m1}(\underset{\sim}{x})] \; d^3\xi_1$$

$$U_{12}(t) = \sum_{i=p,n} \int\rho_1^i(\xi_1) \; V_{k-k} \; (|\underset{\sim}{s}|)\alpha^i\beta^i \; d^3\xi_1 \qquad (8.11)$$

$$U_{13}(t) = \sum_{i=p,n} \int\rho_1^i(\xi_1) \; V_{k-k} \; (|\underset{\sim}{s}|)\alpha^i\beta^i \; \frac{1}{24} \; s^2 d^3\xi_1$$

It is therefore possible to calculate U_{11}, U_{12} and U_{13} for any particular target independant of the projectile type.

The optical potential obtained from equation 8.10 is plotted for ^{3}He, ^{4}He and ^{16}O incident on ^{40}Ca in Fig. 8.1.
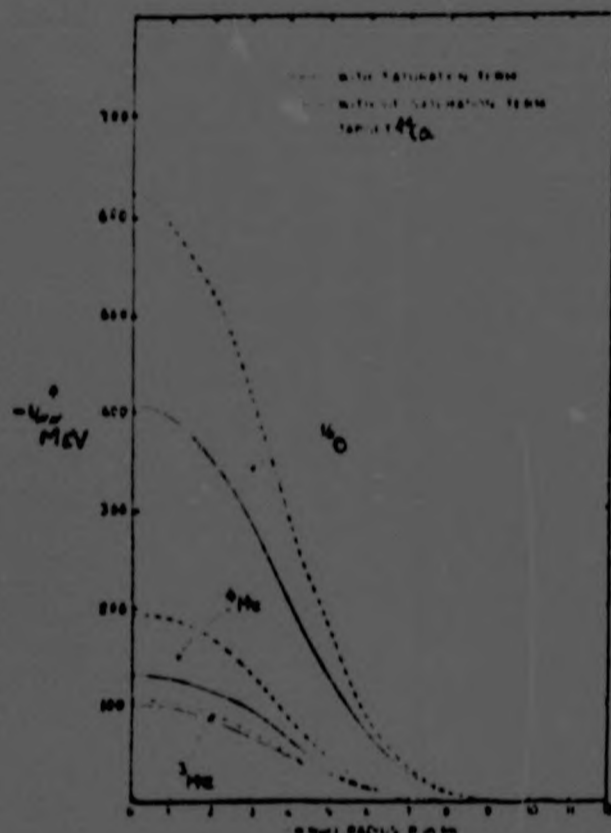

Fig.8.1. The nucleus-nucleus optical potential as a function of R, the distance between the centres of the colliding nuclei.

VIII.4 Use of a Complex Two-Body Interaction

An alternative approach to deriving the nucleus-nucleus optical potential from an effective nucleon-nucleon interaction has been developed by Dover and Vary [33].

The nucleus-nucleus optical potential is written as :

$$V_{opt}(R) = \int d^3r_1 \int d^3r_2 \, \rho_1(\underline{r}_1) \, \rho_2(\underline{r}_2) G \, (\underline{R} + \underline{r}_1 - \underline{r}_2) \qquad (8.12)$$

where ρ_A and ρ_B are the densities of nuclei A and B respectively, and G is the effective nucleon-nucleon interaction.

Assuming a zero-ranged nucleon-nucleon interaction :

$$G \ (\underline{R}+\underline{r}_1-\underline{r}_2) = \gamma \delta^3 \ (\underline{R}+\underline{r}_1-\underline{r}_2) \tag{8.13}$$

we obtain

$$V(\underline{R}) = \gamma \int d^3r_2 \ \rho_1(\underline{r}_2-\underline{R}) \ \rho_2(\underline{r}_2) \tag{8.14}$$

Dover and Vary take γ from the limit of high-energy nucleus-nucleus scattering as :

$$\gamma = -\frac{2\pi\hbar^2}{m} f(0) \tag{8.15}$$

where m is the nucleon mass

and $f(0)$ is the complex forward nucleon-nucleon scattering. This yields the optical potential for the ion-ion interaction

$$V_{opt}(\underline{R}) = -\frac{2\pi\hbar^2}{m} f(0) \int d^3r' \ \rho_1(\underline{r}'-\underline{R}) \ \rho_2(\underline{r}') \tag{8.16}$$

This model was generalized to include the spin and isospin degrees of freedom. The Pauli principle must also be considered as must dispersive and binding effects and the internal Fermi motion of the constituents. The inclusion of these effects results in an improved form of $V_{opt}(R)$, namely :

$$V_{opt}(R) = -\frac{2\pi\hbar^2}{m} \frac{\overline{f(0)}}{(\pi r_0^2)^{3/2}} \int d^3r_1 \int d^3r_2 \ \rho_1(\underline{r}_1)\rho_2(\underline{r}_2)e^{-R^2/r_0^2} \tag{8.17}$$

where r_o is a range parameter and $\bar{F}$ is a complex
depth parameter.

The ansatz for the effective interaction G in equation
8.12 is therefore

$$G = -\frac{2\pi\hbar^2}{m}\, \bar{F}\, N\, e^{-R^2/r_o{}^2} \tag{8.18}$$

where N is a normalization constant.

The two parameters appearing in the complex quantity $\bar{F}$
can then be varied to give a good fit to the elastic
nucleus-nucleus scattering data.

The real and imaginary parts of the folded potential
are illustrated for ^{18}O-^{60}Ni in Fig. 8.2 .

Fig. 8.3 shows the results of a best fit to the ^{18}O-^{60}Ni
angular cross-section data at 62.92 MeV with $\bar{F} = 1.27 + 0.9i$ fm
and to the α-^{208}Pb data at 139 MeV with $\bar{F} = 1.79 + 1.21i$ fm.
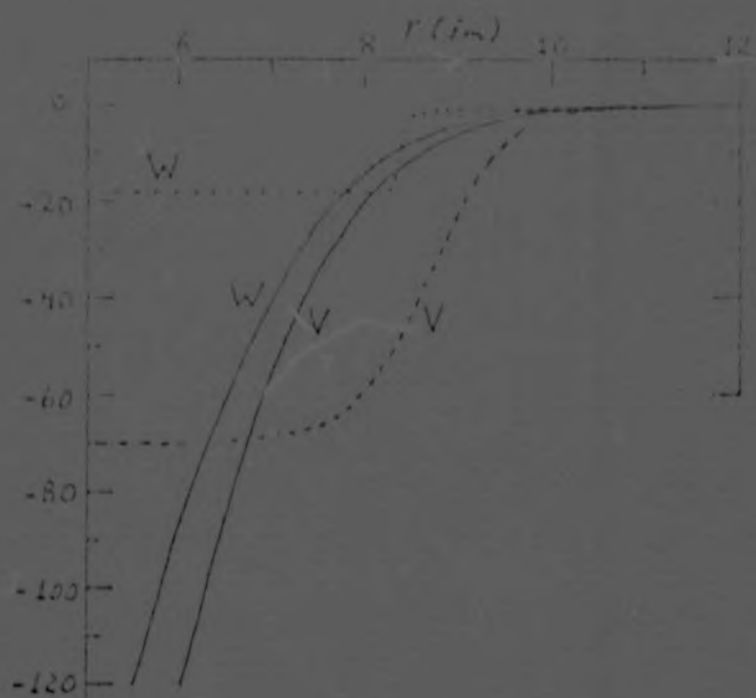
Fig. 8.2. The solid curves V and W are the real and imaginary parts of the folded potential. The dashed curves correspond to Woods-Saxon potentials which yield a good fit to the ^{60}Ni(^{16}O,^{16}O)^{60}Ni reaction.
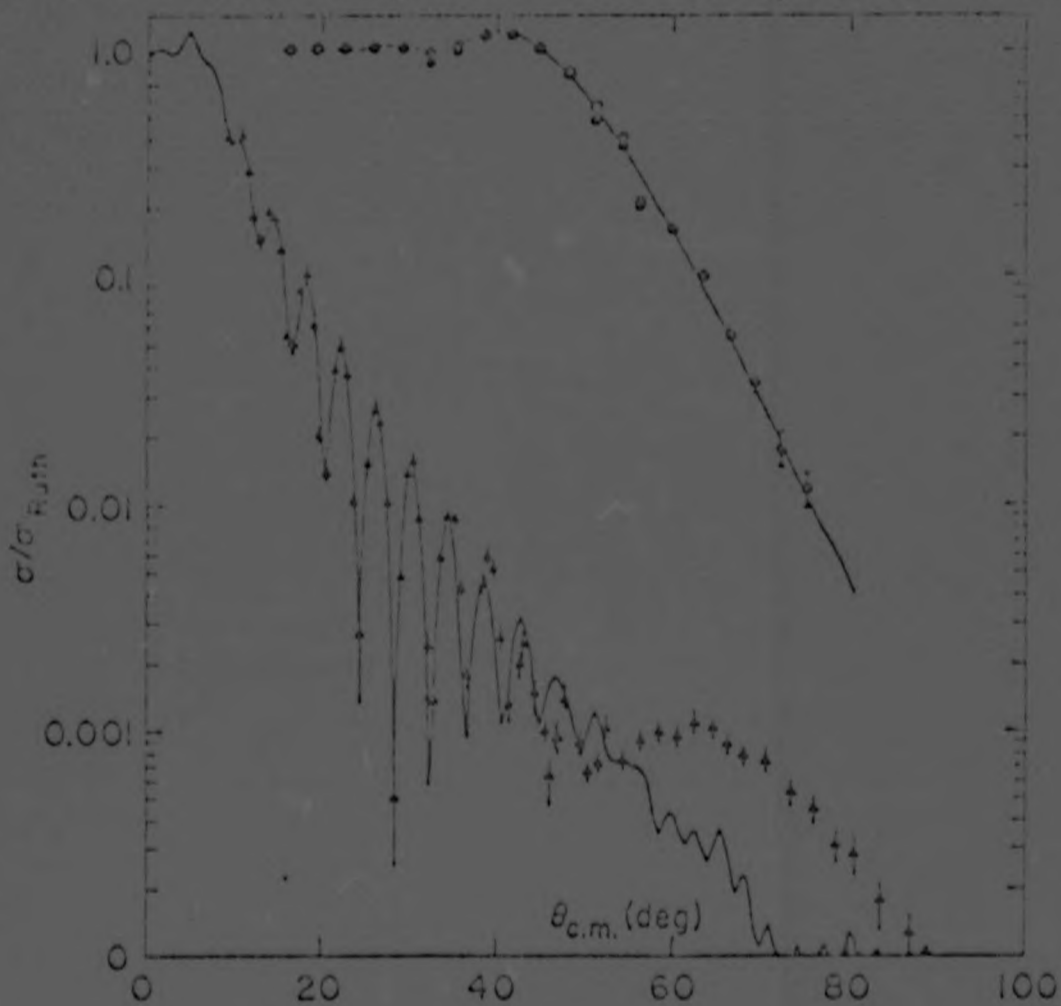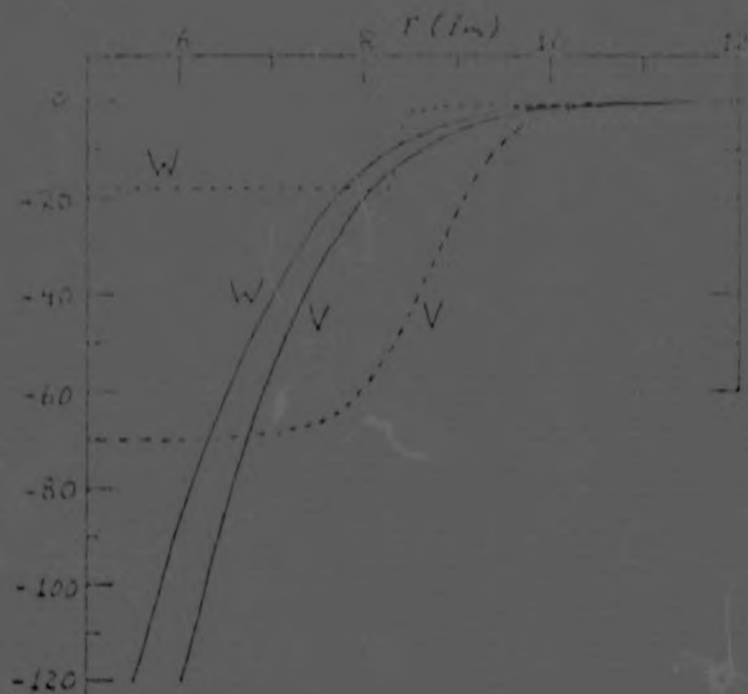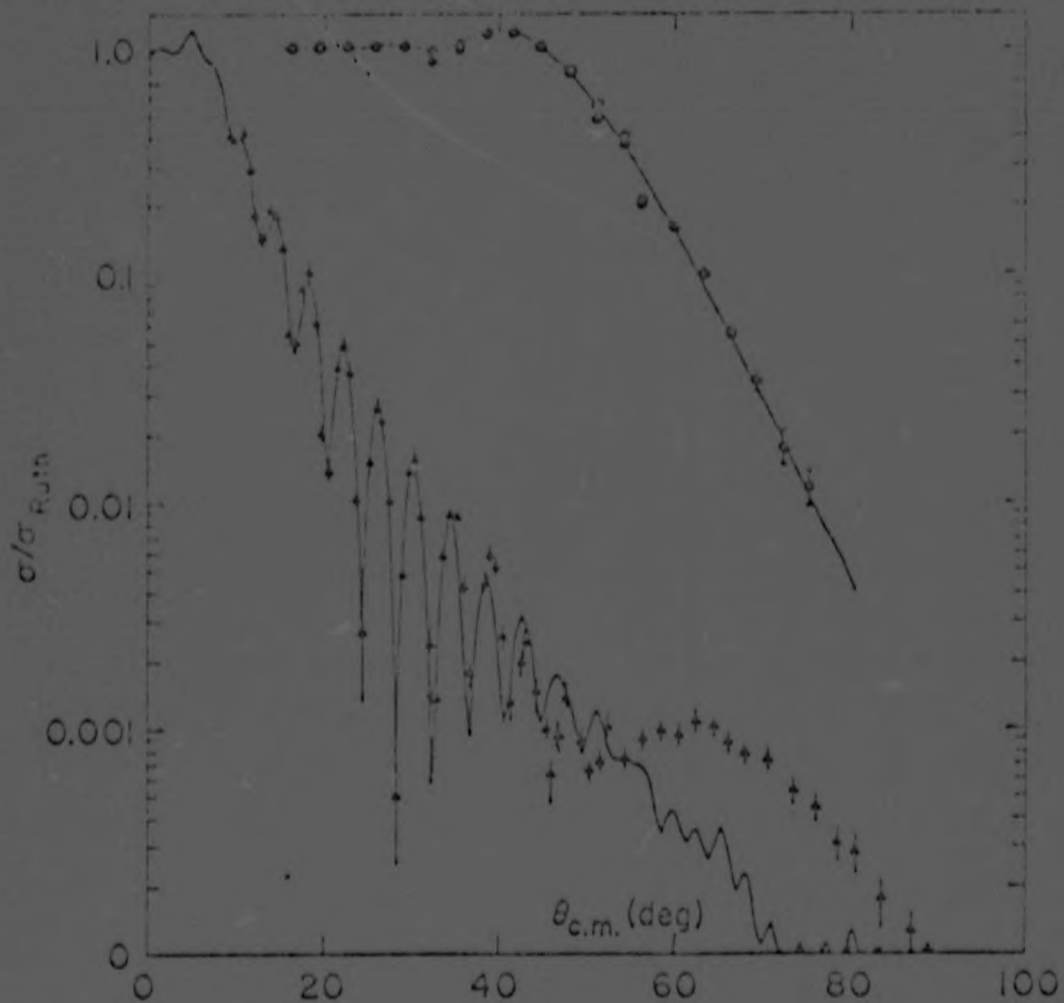

Fig. 8.3. The top curve shows the fit to the Brookhaven ^{16}O+^{60}Ni elastic data at 67.92 MeV with $r = 1.27 + 0.91$ fm. The lower curve displays the fit to the Maryland $\alpha + ^{208}$Pb data at 139 MeV with $r = 1.75 + 1.21$ fm.

Fig. 8.2. The solid curves V and W are the real and imaginary parts of the folded potential. The dashed curves correspond to Woods-Saxon potentials which yield a good fit to the ^{60}Ni(^{12}C,^{16}O)^{62}Ni reaction.

Fig. 8.3. The top curve shows the fit to the Brookhaven ^{16}O+^{60}Ni elastic data at 60.02 MeV with $\bar{r} = 1.27 + 0.91$ fm. The lower curve displays the fit to the Maryland α+^{208}Pb data at 139 MeV with $\bar{r} = 1.75 + 1.21$ fm.

It can be seen that this model provides predictions in
good agreement with experiment. However the concept of a
complex interaction arises in nucleus-nucleus scattering
from the presence of many-body effects and may have
validity for nucleon-nucleon interactions at high energies
where the pion channels are open. For the energies
currently of interest in heavy-ion collisions the concept of
a complex nucleon-nucleon interaction is extremely dubious
and this method can therefore be best regarded as a phenomen-
ological parametrisation.

CHAPTER IX

Energy-Dependant Real Potential

IX.1 Introduction

In the study of heavy-ion scattering using an optical
model, it has been conventional to assume a real potential
which is only dependant on the separation of the nuclei R,
i.e. $V=V(R)$. Following thesuccess enjoyed by the Yale
group in fitting an optical model to the experimental data
(see Chapter III), it has become common for optical model
analyses of heavy-ion experiments to employ a Saxon-Woods
shape for the real potential. However there exists no
a priori reason for believing that the description of the
many-body interaction between two complex nuclei by means
of a two-body, local and ℓ-independant potential having a
Saxon-Woods shape has any fundamental justification.

Theoretical studies have been made to establish the
ℓ-dependance and energy dependance of the imaginary
potential [9],[27]. The collision between two complex
nuclei is also expected to have a non-local behaviour in the
real potential. Now a non-local potential can be expanded
into a local energy-dependant one and it is therefore
proposed to study the energy dependance of the real potential.
Phenomenological energy-dependant real potential fits have
been made for the $^{12}C-^{12}C$ interaction [34]. We will here
attempt a semi-microscopic approach.

In the interaction of two nuclei the real potential acting between the nuclei at any given separation distance R, is considered to be the change in energy of the nuclei in being brought from infinite separation to this separation R. Now the change in energy of the nuclei at any separation R is a summation of the energy shifts for all volume elements in coordinate space. For any given volume element the energy shift can be related to the interaction of the nuclear matter of one nucleus in this element with the nuclear matter of the other nucleus in this element. This interaction can in turn be derived from a consideration of the interaction of two Fermi spheres in momentum space which is dependant on the energy of the relative motion of the two nuclei.

IX.2 The Reaction Matrix

Consider a two-nucleon system with relative momentum of the nucleons k. The system is defined by the initial unperturbed wavefunction ϕ_k for the unperturbed zero order Hamiltonian H_o

$$H_o \phi_k = E_k^o \phi_k \tag{9.1}$$

If a perturbative interaction V is allowed to act between the two nucleons the unperturbed wavefunction ϕ_k will go over to the perturbed wavefunction ψ_k, the ground state wavefunction of the new Hamiltonian $H_o + V$ with corresponding energy $E_k^o + \Delta E$

$$(H_0 + V) \psi_k = (E_k^0 + \Delta E) \psi_k \tag{9.2}$$

ΔE is the energy shift induced by the presence of the interaction V.

Taking the inner product of ψ_k with equation 9.1 and of ϕ_k with equation 9.2 gives the following relationships :

$$E_0 \langle \psi_k | \phi_k \rangle = \langle \psi_k | H_0 | \phi_k \rangle \tag{9.3}$$

$$E_0 \langle \phi_k | \psi_k \rangle + \Delta E \langle \phi_k | \psi_k \rangle = \langle \phi_k | H_0 | \psi_k \rangle + \langle \phi_k | V | \psi_k \rangle \tag{9.4}$$

Assuming ϕ_k and ψ_k satisfy the same boundary condition, then

$$\Delta E \langle \phi_k | \psi_k \rangle = \langle \phi_k | V | \psi_k \rangle$$

which yields for the energy shift

$$\Delta E = \frac{\langle \phi_k | V | \psi_k \rangle}{\langle \phi_k | \psi_k \rangle}$$

Normalizing ψ_k such that $\langle \phi_k | \psi_k \rangle = \langle \phi_k | \phi_k \rangle = 1$ gives :

$$\Delta E = \langle \phi_k | V | \psi_k \rangle \tag{9.5}$$

Defining the g-matrix, also called the reaction matrix, by

$$g \phi_k = V \psi_k$$

the interaction energy for two free nucleons is

$$\Delta E = g_{kk} = \langle \phi_k | V | \psi_k \rangle \tag{9.6}$$

The treatment can be extended to deal with a two-particle interaction in a many body system.

Denoting the eigenfunctions of the Hamiltonian H_0 by ϕ_n the ground state of the system is ϕ_0. When perturbation V is turned on the eigenfunction ψ_0 of the new Hamiltonian

$\emptyset_o$, ψ can be expanded in terms of the original basis wave-
functions

$$\psi_o = \emptyset_o + \sum_{m \neq o} a_m \emptyset_m \tag{9.7}$$

with the normalization condition

$$\langle \emptyset_o | \psi_o \rangle = \langle \emptyset_o | \emptyset_o \rangle = 1 \tag{9.8}$$

Multiplying the Schrodinger equation for the perturbed
system on the left by $\emptyset_m$ and integrating over all space gives :

$$a_m E_m^o + \langle \emptyset_m | V | \psi_o \rangle = a_m E \tag{9.9}$$

Thus

$$\psi_o = \emptyset_o - \sum_{m \neq o} \frac{\langle \emptyset_m | V | \psi_o \rangle}{E_m^o - E} \emptyset_m \tag{9.10}$$

The energy denominator $E_m^o - E$ is denoted by e_m.
Defining

$$G\emptyset_o = V\psi_o \tag{9.11}$$

gives

$$\Delta E = \langle \emptyset_o | V | \psi_o \rangle = \langle \emptyset_o | G | \emptyset_o \rangle \tag{9.12}$$

For two interacting particles in nuclear matter the
sum over m in 9.10 must be restricted to states in which
both particles lie outside the Fermi sea in order to satisfy
the Pauli exclusion principle. This can be done by means
of a Pauli projection operator Q; it is 1 if both states
are empty and zero otherwise. Then

$$\Delta E = \langle \psi_k | G | \psi_k \rangle$$
$$= V_{kk} - \sum_m \frac{G_{km} V_{mk}}{e_m} \quad G_{mk} \tag{9.13}$$

This can be written formally as

$$G = V - V \frac{Q}{e} G \tag{9.14}$$

This can be compared to the corresponding expression for the free reaction matrix t, namely

$$t = V - V \frac{1}{e} t \tag{9.15}$$

Thus the interaction energy for two nucleons of relative momentum k bound in nuclear matter is

$$\Delta E = G_{kk}$$

where G satisfies the integral equation 9.14

IX.3 The Density Distribution

We now consider the situation in coordinate space for colliding heavy-ions. We schematically consider when the two nuclei, assumed to have Saxon-Woods distribution of nucleon density, begin to overlap (Fig. 9.1)
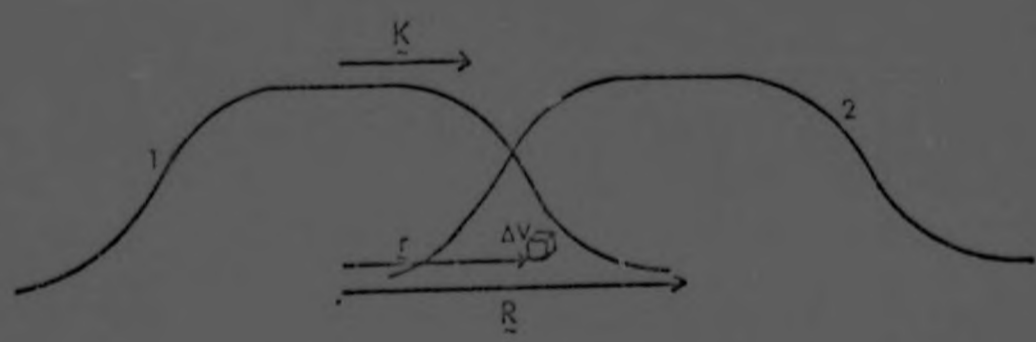

Fig. 9.1. Density distribution for nuclei separated by distance R.

$$W = \langle ? | ? | ? \rangle$$
$$= V_{} - \sum_{?} \frac{?_? V_{??}}{?_?} \; ?_{??} \qquad (9.13)$$

This can be written formally as

$$G = V - V \frac{?}{e} G \qquad (9.14)$$

This can be compared to the corresponding expression for the free reaction matrix g, namely

$$g = V - V \frac{1}{e} g \qquad (9.15)$$

Thus the interaction energy for two nucleons of relative momentum k bound in nuclear matter is

$$\Delta E = G_{kk}$$

where G satisfies the integral equation 9.14

IX.3 The Density Distribution

We now consider the situation in coordinate space for colliding heavy-ions. We schematically consider when the two nuclei, assumed to have Saxon-Woods distribution of nucleon density, begin to overlap (Fig. 9.1)

Fig. 9.1. Density distribution for nuclei separated by distance R.

Fig. 9.1 depicts the situation when the separation of the two nuclear centres is R and the nuclei have relative momentum K per nucleon. At volume element ΔV we can associate a nucleon density $\rho(r_1)$ from nucleus 1 and a nucleon density $\rho(r_1-R)$ from nucleus 2.

The Saxon-Woods distribution for nuclear matter in the nucleus i, is of the form

$$\rho_i(r) = \frac{\rho_{0i}}{1 + \exp(|r|-C_i)/b_i} \tag{9.16}$$

where $\rho_{0i} = 3A_i\left(4\pi C_i^3\left[1+\left(\frac{\pi b_i}{C_i}\right)^2 + 6\left(\frac{b_i}{C_i}\right)^3 e^{-C_i/b_i}\right]\right)^{-1}$ (9.17)

C_i is the diffuseness parameter

and b_i is the radius parameter

A_i is the nucleon number.

Therefore at any point r, when the nuclei have separation R, the densities for the two nuclei will be given by :

$$\rho_1(r) = \frac{\rho_{01}}{1 + \exp\dfrac{(|r|-C_1)}{b_1}} \tag{9.18}$$

and $\rho_2(r) = \dfrac{\rho_{02}}{1 + \exp\dfrac{(|r-R|-C_2)}{b_2}}$

The identification of nuclear matter in the overlap region with a specific nuclear centre is a dubious procedure. A more rigorous approach should include a treatment of the antisymmetrization requirements for the overlapping nuclei. As the degree of overlap increases it is less and less justified to neglect antisymmetrization. The cross-section however is more sensitive to the shape and nature of the

potential at the surface where the degree of overlap is still relatively small. For the regions of small overlap the Pauli exclusion principle is still expected to give a small effect. We therefore aim to derive an energy dependance of the real potential with values of which we can be confident in the region where overlap begins.

In any volume element the nucleons are not expected to remember which nucleus originally carried them into the collision and instead of associating the densities ρ_1 with nucleus 1 and ρ_2 with nucleus 2 one can improve the treatment by considering a compound density for the system. This can be done in the extreme limits of either the sudden or adiabatic approximations.

We then have at a point $\underset{\sim}{r}_1$ from the centre of nucleus 1 a compound density $\rho_{C.D.}$, given by

$$\rho_{C.D.} = \rho_1(\underset{\sim}{r}_1) + \rho_2(\underset{\sim}{r}_1 - \underset{\sim}{R}) \tag{9.19}$$

when the nuclei are separated by a distance $\underset{\sim}{R}$. This compound density is then ascribed to nucleus i with a density of states $\dfrac{\rho_i}{\rho_{C.D.}}$

We now have to determine the energy of interaction in volume element ΔV between two nuclei where nucleus 1 has momentum $\underset{\sim}{K}$ per nucleon relative to nucleus 2. A consideration of the problem in momentum space is facilitated by the Thomas-Fermi theory of nuclear matter, in which a Fermi-momentum k_F is locally associated with the density ρ.

IX.4 The Density-Momentum Relation

Consider the simplified situation of an arbitrary, one-dimensional potential $V(x)$. Assume that for x Consider the simplified situation of an arbitrary1 attains a constant value $V(x) = -V_o$ (9.20)

The potential is also assumed to have the properties

$$\frac{dV}{dx} \leq 0 \text{ for all x}$$

and $V(o) = 0$

All states in this potential having energy $E<0$ are assumed to be occupied and states with $E>0$ are assumed to be empty. This corresponds to a Fermi energy $E_F=0$. Should the Fermi potential not be equal to zero the treatment could be modified by adding a constant E_F to both E and V.

The wave functions can be treated to good approximation over most of the range of x by the W.K.B. method. The wave functions in the potential 9.20 are

$$\psi = \emptyset(x) \exp i \underset{\sim}{k'} \underset{\sim}{r} \qquad (9.21)$$

where $\underset{\sim}{k'}$, the "perpendicular momentum", is a vector in the y,z plane.

Then $\emptyset$ satisfies

$$-\frac{\hbar^2}{m} \emptyset'' + (2E - 2V(x) -\frac{\hbar^2}{m} k'^2) \emptyset = 0 \qquad (9.22)$$

Define $\frac{\hbar^2}{m} k_x^2 = 2E-2V(x) - \frac{\hbar^2}{m} k'^2$ (9.23)

$\frac{\hbar^2}{m} k_{x_o}^2 = 2E-2V_o -\frac{\hbar^2}{m} k'^2$ (9.24)

For any given energy E, k' must satisfy

$$\frac{\hbar^2}{m} k'^2 < 2(E-V_0) \quad \text{in order to fulfil the}$$

condition $\frac{\hbar^2}{m} k_{x_0}^2 > 0$

$\emptyset(x)$ is a standing wave which can be normalized
by requiring

$$\emptyset \rightarrow \sqrt{2} \cos (k_{x_0} x + \alpha) \text{ as } x \rightarrow \infty$$

and implies that the average density inside the
nucleus goes to unity. The W.K.B. approximation is good
for $k_x^2 > 0$. For this region of space $\emptyset(x)$ is given by

$$\emptyset(x) = \sqrt{\frac{2k_{x_0}}{k_x(x)}} \cos (\int^x k_x(x')dx' + \beta)$$

$$\emptyset(x) = \sqrt{2k_{x_0}} \, \emptyset_1 (k_{x_0},x) \tag{9.25}$$

The total density is then

$$\rho(x) = \frac{4}{(2\pi)^3} \int_0^{k_{FO}} d^3k_0 \, |\psi(k_{x_0},k_y,k_z;x)|^2 \tag{9.26}$$

$$= (2\pi^3)^{-1} \int_0^{k_{FO}} 2dk_{x_0} \int^{(k_{FO}^2-k_{x_0}^2)} d(k'^2)\pi |\psi(k_{x_0};x)|^2$$

$$= \frac{1}{2\pi^2} \int_0^{k_{FO}} 2dk_{x_0} \int^{k_{FO}^2-k_{x_0}^2} \emptyset^2(x) \, d(k'^2)$$

From 9.25

$$\rho(x) = \frac{1}{2\pi^2} \int_0^{k_{FO}} 2dk_{x_0} \int^{k_{FO}^2-k_{x_0}^2} 2k_{x_0} \emptyset_1^2 (k_{x_0};x) \, d(k'^2)$$

$$= \frac{1}{\pi^2} \int_0^{k_{FO}} 2k_{x_0} dk_{x_0} (k_{FO}^2-k_{x_0}^2) \, \emptyset_1^2 (k_{x_0};x)$$

$$= \frac{1}{\pi^2} \int_0^{k_{FO}} (k_{FO}^2-k_{x_0}^2) \, \emptyset_1^2 (k_{xo};x) \, d(k_{x_0}^2) \tag{9.27}$$

Now for $k_x^2(x) > 0$ we average the $\cos^2$ factor in $\emptyset_1^2$ to give $\frac{1}{2}$. When $k_x^2 < 0$ we set $\emptyset_1 = 0$. Now from 9.23 and 9.24 we have :

$$k_x^2 = k_{x_0}^2 - \text{const.} \qquad \text{for fixed x.}$$

Therefore 9.27 becomes

$$\rho(x) = \pi^{-2} \int_0^{k_F^2(x)} [k_F^2(x) - k_x^2(x)] \frac{1}{2k_x} d(k_x)^2$$

$$= \left(\frac{2}{3} \pi^2\right)^{-1} k_F^3 \tag{9.28}$$

This expression must be corrected for the presence of the inhomogeneous surface region [14]. The corrected expression gives :

$$k_F^2(r) = [3\pi^2\rho(r)]^{2/3} \{[\tfrac{1}{2}(1-\alpha)]^{5/3} + [\tfrac{1}{2}(1+\alpha)]^{5/3}\}$$

$$+ \frac{5}{12} \xi \left(\frac{\nabla\rho}{\rho}\right)^2 \tag{9.29}$$

where $\alpha = \dfrac{N-Z}{N+Z}$ is the neutron excess parameter

and ξ was chosen in Ref. (14) to have the value $\xi = \dfrac{1}{9}$.

Assuming a Saxon-Woods shape for the nucleon distribution we have for the compound density

$$\rho_{C.D.} = \rho_1 + \rho_2$$

$$= \frac{\rho_{01}}{1 + \exp\dfrac{|r| - C_1}{b_1}} + \frac{\rho_{02}}{1 + \exp\dfrac{|r-R| - C_2}{b_2}}$$

$$|r| = \sqrt{x^2 + y^2 + z^2}$$

In cylindrical coordinates (α, θ, Z), where $\alpha = \sqrt{x^2 + y^2}$ and Z is the direction of the axis joining the two nuclear centres, we have

$$(\nabla \rho_{C.D})^2 = \left(\frac{\partial \rho_{C.D}}{\partial Z}\right)^2 + \left(\frac{1}{\alpha}\frac{\partial \rho_{C.D}}{\partial \theta}\right)^2 + \left(\frac{\partial \rho_{C.D}}{\partial \alpha}\right)^2$$

$$= \left(\frac{\partial \rho_{C.D}}{\partial Z}\right)^2 + \left(\frac{\partial \rho_{C.D}}{\partial \alpha}\right)^2 \qquad (9.30)$$

where $\rho_{C.D} = \dfrac{\rho_{01}}{1+\exp\left(\dfrac{\sqrt{Z^2+\alpha^2}-C_1}{b_1}\right)} + \dfrac{\rho_{02}}{1+\exp\left(\dfrac{\sqrt{Z^2+(\alpha-R)^2}-C_2}{b_2}\right)}$

$$(9.31)$$

Denoting $\exp\left(\dfrac{\sqrt{Z^2+\alpha^2}-C_1}{b_1}\right)$ by E_1

and $\exp\left(\dfrac{\sqrt{Z^2+(\alpha-R)^2}-C_2}{b_2}\right)$ by E_2 we have

$$\frac{\partial \rho_{C.D}}{\partial Z} = -\left[\frac{\rho_{01}}{b_1}\frac{Z}{\sqrt{Z^2+\alpha^2}}\frac{E_1}{(1+E_1)^2} + \frac{\rho_{02}}{b_2}\frac{Z}{\sqrt{Z^2+(\alpha-R)^2}}\frac{E_2}{(1+E_2)^2}\right]$$

$$(9.32)$$

$$\frac{\partial \rho_{C.D}}{\partial \alpha} = -\left[\frac{\rho_{01}}{b_1}\frac{\alpha}{\sqrt{Z^2+\alpha^2}}\frac{E_1}{(1+E_1)^2} + \frac{\rho_{02}}{b_2}\frac{(\alpha-R)}{\sqrt{Z^2+(\alpha-R)^2}}\frac{E_2}{(1+E_2)^2}\right]$$

$$(9.33)$$

Expressions 9.30, 9.32 and 9.33 can be substituted into equation 9.29 for the inhomogeneity correction.

Since a density can be associated with any point in coordinate space for each of the colliding nuclei we are able to determine the region occupied in momentum space

for each point in coordinate space.

IX.5   Momentum Space Considerations

The value of the local relative momentum per nucleon K arising from the relative motion of the nuclear centres determines the separation in momentum space of the two Fermi spheres associated with the density distribution at a point.   For two colliding nuclei, atomic number A, incident on one another with energy $E_{C.M.}$ in the centre-of-mass frame of reference, the relative momentum per nucleon, K, is given by

$$\frac{\hbar^2}{m} \; (AK)^2 = E_{C.M.}$$

or $K = \dfrac{\sqrt{mE_{C.M.}}}{A\hbar}$ (9.34)

where m is the nucleon mass.

To determine the relative momentum per nucleon for a given separation distance $\underline{R}$, we replace $E_{C.M.}$ by $(E_{C.M.} - V_T(\underline{R}))$

in equation 9.34, where $V_T(\underline{R})$ is the total nucleus-nucleus potential at that separation distance.   (Fig. 9.2) :
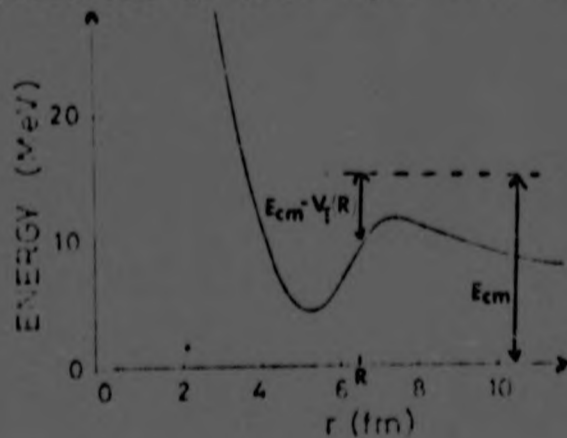
Fig. 9.2.   Illustration of the local energy

If we adopt the approach that at every point we determine the Fermi momentum of nucleus 1 only from its own nucleon distribution and similarly for nucleus 2, then a number of different situations arise in momentum space. These are illustrated below
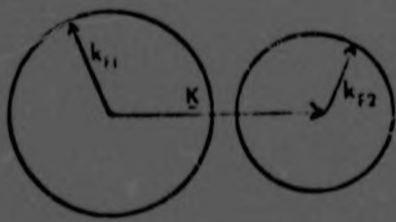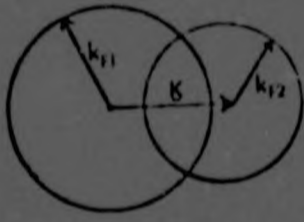

Fig. 9.3a. $k_{F1} + k_{F2} < k$ Fig. 9.3b. $k_{F1} \leq k_{F2} + K$ Fig. 9.3c. $k_{F2} + K < k_{F1}$

$k_{F1} + k_{F2} > K$ $k_{F2} < K$

Various other cases arise but do not yield different final expressions. For example an equivalent case to Fig. 9.3c is shown below

Fig.9.4. $k_{F2} + K < k_{F1}$

$k_{F2} > K$

The use of a compound density to describe the density distribution implies that $k_{F1} = k_{F2}$ always. This is merely

a special situation for the various cases above.

We recall that we wish to calculate the energy of
~~a special situation for the various cases above~~ between two
nuclei having relative momentum K per nucleon. Depending
on the density distribution at the particular point in
question this is equivalent to calculating the interaction
energy between the two Fermi spheres in one of the cases
illustrated in Fig. 9.3. We thus have the interaction
energy density $\frac{\Delta E}{\Delta V} = \varepsilon(k_{F1}, k_{F2}, K)$ where $k_{Fi} = k_{Fi}(\underline{R}, \underline{r})$, $i = (1,2)$

Using the compound density approach

$$\varepsilon(k_{F1}, k_{F2}, K) = \frac{1}{(\Delta v)^2} \frac{\rho_1}{\rho_{C.D}} \frac{\rho_2}{\rho_{C.D}} \int_{F1} \int_{F2} G_{kk} \, d^3k_1 \, d^3k_2$$

(9.35)

where Δv is the normalization volume,

F_1 and F_2 denote the volume occupied by Fermi spheres
1 and 2 respectively.

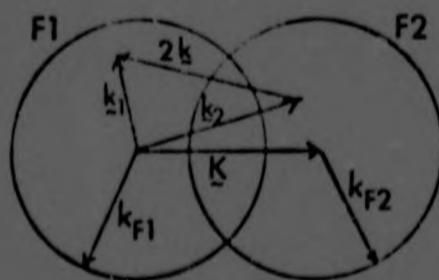The relative momentum $\underline{k}$ is illustrated in Fig. 9.5

Fig. 9.5. Fermi spheres F1 and F2 in momentum
space.

A calculation of the interaction energy density requires
some functional form for the reaction matrix G_{kk}. As a first
approach we will consider the problem in phase shift approximation.

Author Saloner D A
Name of thesis A semi-microscopic calculation of the potential in heavy ion collisions 1975